$Nef_{JR\text{-}CSF}$ and $Nef_{NL4\text{-}3}$ (Figure 2).

Altogether, it was indicated that the extreme difference in expression level between $Nef_{JR\text{-}CSF}$ and $Nef_{NL4\text{-}3}$ is not due to experimental artifacts but due to the property of each Nef. Furthermore, the diversity of the Nef expression level is plausible, although more Nef clones should be examined to draw an unequivocal conclusion. Previously, Hartz et al. have reported that Nef from the HIV-1_{lai} strain shows a low expression level in COS-1 cells [33], although they have not evaluated relative expression levels among some Nef variants. At the least, a considerable difference in the level between $Nef_{NL4\text{-}3}$ and $Nef_{JR\text{-}CSF}$ in HEK293 cells was confirmed in these experiments.

To confirm whether both $Nef_{NL4\text{-}3}$ and $Nef_{JR\text{-}CSF}$ expressed in HEK293/CD4 cells are functional, their CD4 downregulation activitiy, which is the main function of Nef, were evaluated. As shown in Figure 3, the CD4 downregulation activities of $Nef_{NL4\text{-}3}$ and $Nef_{JR\text{-}CSF}$ were clearly observed. The activity of $Nef_{NL4\text{-}3}$ was less than that of $Nef_{JR\text{-}CSF}$, in which the mean fluorescent intensities (MFIs) indicating the CD4 level in two $Nef_{NL4\text{-}3}$-expressing cell clones were 0.65 and 0.63, whereas those in two $Nef_{JR\text{-}CSF}$ expressing cell clones were 0.18 and 0.12. The *N*-myristoylation at the *N*-terminus of Nef is essential for the CD4 downregulation activity [2]. To verify thether CD4 downregulation in HEK293/CD4 cells is induced by the expressed Nefs, clones of HEK293/CD4 cells expressing non-myristoylated G2A mutants of $Nef_{NL4\text{-}3}$ or $Nef_{JR\text{-}CSF}$ were established and the CD4 levels were evaluated. Each G2A non-myristoylated mutant of $Nef_{NL4\text{-}3}$ or $Nef_{JR\text{-}CSF}$ expectedly showed no CD4 downregulation. It is clear that both $Nef_{NL4\text{-}3}$ and $Nef_{JR\text{-}CSF}$ are certainly functional in HEK293/CD4 cells and that a high expression level of Nef is associated with efficient CD4 downregulation.

Characterization of low expression property of Nef

To determine which region of $Nef_{NL4\text{-}3}$ is responsible for the low expression level, a chimera Nef expression vector was constructed. The primary structure of the chimera Nef tested was as follows: the first half-sequence, amino acids (AA) 1-139, was from $Nef_{JR\text{-}CSF}$ and the second half-sequence, AA129-206, was from $Nef_{NL4\text{-}3}$ (Figure 4A). HEK293 cells were transfected with each Nef expression vector and subjected to western blot analysis. As shown in Figure 4B, the expression level of the chimera Nef was almost the same as that of $Nef_{NL4\text{-}3}$. According to the quantification of the intensities of the bands with Fujifilm Image Gauge Software, the expression level of the chimera Nef was about 10% of that of $Nef_{JR\text{-}CSF}$. This result suggests that AA129-206 of $Nef_{NL4\text{-}3}$, named NLAA129-206, is required for the low expression level.

To examine whether the NLAA129-206 is not only required but also sufficient for the induction of the low protein expression level, the region was appended to the *C*- or *N*-terminal end of the enhanced green fluorescent protein (EGFP) [34, 35]. We used the combination of two protein degradation sequences, CL1 and PEST [12, 15, 36], namely, the CP sequence as a positive control of the induction of the low protein expression level. The CP sequence can induce a strong proteasome-mediated protein degradation by fusion, resulting in a low protein expression level [17, 37]. Since the PEST sequence can induce protein degradation by fusion to the *C*- or *N*-terminal end of target proteins [16], we appended the NLAA129-206 to the *C*- or *N*-terminal end of EGFP (Figures 4C). The $(GGGGS)_3$ linker was inserted between EGFP and each appended amino acid sequence (Figures 4C). It has been reported that the linker is sufficiently long and flexible to retain the function of two proteins at both ends [27]. HEK293 cells were transiently transfected with the each expression vector and cultured for 48 h. Each cellular lysate was subjected to western blot analysis as described in Materials and Methods. As shown in Figures 4D and E, the expression levels of the NLAA129-206-fused EGFPs were extremely lower than that of wild-type EGFP in the *C*- and *N*-terminal fusions. Furthermore, the expression levels of the EGFPs fused by NLAA129-206 were clearly lower than those of the EGFP fused by the CP sequence (Figures 4D and E). The β-actin levels were almost the same among the lines, showing that the amounts of loaded proteins were almost the same among the lines. Another very small band in addition to the main one was observed in EGFP (asterisk in Figure 4D), which is not identified but thought to be EGFP with posttranslational modifications. These results suggest that NLAA129-206 has a very high potential for inducing the low protein expression level by fusion. Additionally, the potential of NLAA129-206 seems to be brought out more effectively in the case of fusion to the *N*-terminal end of EGFP than in the case of fusion to the *C*-terminal end of EGFP.

To examine whether the induction of the low protein expression level by the fusion of the sequence occurs in not only EGFP but also other proteins, Rluc [29] was chosen for the experiment. Since the fusion of NLAA129-206 to the *N*-terminal end of EGFP was more effective than that to the *C*-terminal end for the induction of the low protein expression level (Figures 4D and E), the NLAA129-206 and CP sequences were appended to the *N*-terminal of Rluc for examination (Figure 4C). The expression level of Rluc could be evaluated by measuring bioluminescent activity [29]. Transiently, HEK293 cells expressing each Rluc were lysed and their Rluc activity was measured, as described in Materials and Methods. As shown in Figure 4F, the activity of NLAA129-206-fused Rluc was much lower than that of not only wild-type Rluc but also CP-fused Rluc, whose results were identical to those of EGFP (Figures 4D and E). These results suggest that the induction

of the low protein expression level by NLAA129-206 fusion universally occurs in all arbitrary proteins.

To investigate the minimum sequence of NLAA129-206 for inducing the low protein expression level, the expression levels of the three deletion mutants (NLAA142-206, NLAA129-186, and NLAA142-186) shown in Figure 5A were examined. HEK293 cells were transiently transfected with each expression vector and cultured for 48 h. Each cellular lysate was subjected to western blot analysis for EGFP fusion proteins and to the measurement of bioluminescent activity for Rluc fusion proteins, as described in Materials and Methods. As shown in Figure 5B, partial recovery of the expression levels was observed in both the N- and *C*-terminal-region-deleted mutants, namely, NLAA142-206-EGFP and NLAA129-186-EGFP, respectively. The *N*- and *C*-terminal-region-deleted mutant NLAA142-186-EGFP showed almost full recovery of its expression level, similarly to the original EGFP. Almost identical profiles of the expression pattern in Figure 5B were observed in the comparison of activity among the deletion-mutant-fused Rluc's (Figure 5C). These results suggest that the complete sequence of NLAA129-206 is required for the induction of the lowest protein expression level. It is thought that the stepwise reduction levels established by the attachment of NLAA129-206 and the mutants would become a useful repertory for inducing the desired expression of arbitrary proteins.

The NLAA129-206 regions of the Nef_{NL4-3}-corresponding sequences of Nef_{JR-CSF} and Nef_{mac239} were named JRAA139-216 and macAA161-263, respectively. The expression levels of Nef_{JR-CSF} and Nef_{mac239} were high among the five Nef's (Figure 1A). Hence, do the JRAA139-216 or macAA161-263 fusion proteins also show relatively high expression levels? The sequence-fused EGFP and Rluc (Figure 6A) expression levels were respectively examined by western blot analysis and Rluc assay. As shown in Figures 6B and C, unexpectedly, but interestingly, JRAA139-216- or macAA161-263-fused EGFP and Rluc also showed extremely low expression levels as in the cases of NLAA129-206. These results suggest that all Nef variants generally have an extremely low expression property in the *C*-terminal region. Since the chimera Nef, i.e., AA1-139 of Nef_{JR-CSF} plus NLAA129-206, showed a low expression level similarly to that of Nef_{NL4-3} (Figures 4B), it is also speculated that the contribution of AA1-139 of Nef_{JR-CSF} to the entire Nef stabilization could be restrictive to the combination of JRAA139-216.

The case with the $(GGGGS)_3$ linker resulted in a much lower expression level of EGFP by the fusion of NLAA129-206 than the case without the linker (data not shown), suggesting that the independence of NLAA129-206 from EGFP generated by the flexibility of the linker is important for the induction of the low expression level. Taking this result into consideration, JRAA139-216 might not show independence from AA1-139 of Nef_{JR-CSF} or express the potential ability to induce the low expression level, which may result in a high expression level of Nef_{JR-CSF}.

Since macAA161-263 could also induce extremely low expression levels of both EGFP and Rluc, the low expression property might be universal in Nef of not only HIV-1 but also SIV. The examination of a more comprehensive set of Nef variants might be necessary to unequivocally conclude the low expression property of the *C*-terminal region of Nef.

Examination of the mRNA levels and effect of proteasome inhibitor on the expression levels

What is the mechanism underlying the induction of the low protein expression level by the fusion of NLAA129-206? First, the mRNA level in HEK293 cells transfected with each DNA was quantified by reverse-transcription real-time quantitative PCR analysis [38]. mRNA level was normalized to the transcript of the neomycin resistance gene, which is coded in the expression vector used. Almost comparable mRNA levels between Nef_{NL4-3} and Nef_{JR-CSF}, or among EGFP, NLAA129-206 fused EGFP, and CP-fused EGFP, were observed (Figures 7A and B). These results suggest that mRNA level cannot be associated with the induction of the extremely low protein expression level.

Then, we examined protein stability. The ubiquitin proteasome system (UPS) is one of the major protein degradation machineries in eukaryotic cells [39]. Nef_{NL4-3}- or NLAA129-206-EGFP-expressing HEK293 cells were treated with the proteasome inhibitor MG132 at 20 μM for 0, 3, or 6 h. The expression level at each time point was measured by western blot analysis, which was normalized to the actin level. As shown in Figures 8A and B, increases in the apparent expression level of both proteins were slightly observed upon treatment with the inhibitor in a time-dependent manner. The results suggest that the low protein expression property of NLAA129-206 may be in part due to a high rate of protein degradation mediated by the proteasome. However, it still cannot be concluded whether the mechanism for the induction of low protein expression level is associated with protein degradation rate, since such proteasome-mediated degradation may generally occur in proteins [39]. There could be other mechanisms of inducing the low protein expression level by the *C*-terminal region of Nef. Now, we are investigating to obtain conclusive evidence from the view point of not only protein destabilization but also protein translation.

Finally, we propose that the NLAA129-206 of Nef_{NL4-3} and the corresponding regions of other Nef variants, at least from HIV-1_{JR-CSF} and SIV_{mac239}, are excellent tools for inducing extremely low expression levels of arbitrary proteins by attachment as fusion proteins. Furthermore, Nef variants from HIV and SIV viruses that are

very rich in genetic diversity may become useful resources for the search of regions inducing low protein expression levels. Such induction of extremely low protein expression levels is applicable to the development of highly responsive reporter systems [18, 19, 26], to the improvement in recombinant protein productivity [19], and to other technological research.

Acknowledgments

We thank Dr. R. Swanstrom (University of North Carolina at Chapel Hill) for helpful discussions. We thank Dr. Shinya Suzu for his kind gift of the HEK239/CD4 cells.

Funding

This study was supported in part by a Grant-in-Aid for Young Scientists from the Ministry of Education, Culture, Sports, Science and Technology of Japan and a Health and Labour Sciences Research Grant from the Ministry of Health, Labour and Welfare of Japan.

References

1. Geyer, M., Fackler, O. T. and Peterlin, B. M. (2001) EMBO Rep. **2**, 580-585
2. Fackler, O. T., Moris, A., Tibroni, N., Giese, S. I., Glass, B., Schwartz, O. and Krausslich, H. G. (2006) Virology. **351**, 322-339
3. Jere, A., Fujita, M., Adachi, A. and Nomaguchi, M. (2010) Microbes Infect. **12**, 65-70
4. Guy, B., Kieny, M.P., Riviere, Y., Le, Peuch. C, Dott, K., Girard, M., Montagnier, L., Lecocq, J.P. (1987) Nature. **330**, 266-269
5. Tebit, D. M., Nankya, I., Arts, E. J. and Gao, Y. (2007) AIDS Rev. **9**, 75-87
6. Berger, E. A., Doms, R. W., Fenyo, E. M., Korber, B. T., Littman, D. R., Moore, J. P., Sattentau, Q. J., Schuitemaker, H., Sodroski, J. and Weiss, R. A. (1998) Nature. **391**, 240
7. Taylor, B. S., Sobieszczyk, M. E., McCutchan, F. E. and Hammer, S. M. (2008) N Engl J Med. **358**, 1590-1602
8. de Sousa Abreu, R., Penalva, L. O., Marcotte, E. M. and Vogel, C. (2009) Mol Biosyst. **5**, 1512-1526
9. Lu, P., Vogel, C., Wang, R., Yao, X. and Marcotte, E. M. (2007) Nat Biotechnol. **25**, 117-124
10. Reinstein, E. and Ciechanover, A. (2006) Ann Intern Med. **145**, 676-684
11. Bachmair, A., Finley, D. and Varshavsky, A. (1986) Science. **234**, 179-186
12. Rogers, S., Wells, R. and Rechsteiner, M. (1986) Science. **234**, 364-368
13. Gilon, T., Chomsky, O. and Kulka, R. G. (1998) EMBO J. **17**, 2759-2766
14. Zhang, M., MacDonald, A. I., Hoyt, M. A. and Coffino, P. (2004) J Biol Chem. **279**, 20959-20965
15. Li, X., Zhao, X., Fang, Y., Jiang, X., Duong, T., Fan, C., Huang, C. C. and Kain, S. R. (1998) J Biol Chem. **273**, 34970-34975
16. Loetscher, P., Pratt, G., Rechsteiner, M. (1991) J Biol Chem. **266**, 11213-11220
17. Fan, F., Wood, K. V. (2007) Assay Drug Dev Technol. **5**, 127-136
18. Voon, D. C., Subrata, L. S., Baltic, S., Leu, M. P., Whiteway, J. M., Wong, A., Knight, S. A., Christiansen, F. T. and Daly, J. M. (2005) Nucleic Acids Res. **33**, e27
19. Leclerc, G. M., Boockfor, F. R., Faught, W. J. and Frawley, L. S. (2000) Biotechniques. **29**, 590-591, 594-596, 598 passim
20. Paguio, A., Stecha, P., Wood, K. V. and Fan, F. (2010) Curr Chem Genomics. **4**, 43-49
21. Ng, S. K., Wang, D. I. and Yap, M. G. (2007) Metab Eng. **9**, 304-316
22. Zubiaga, A.M., Belasco, J.G., Greenberg,M. E. (1995) Mol. Cell. Biol. **15**, 2219–2230
23. Yeilding, N. M., Rehman, M. T. Lee, W. M. (1996) Mol. Cell. Biol. **16**, 3511–3522
24. Shyu, A. B., Greenberg, M. E. and Belasco, J. G. (1989) Genes Dev. **3**, 60–72
25. Laguette, N., Benichou, S., Basmaciogullari, S. (2009) J Virol. **83**, 1093-1104
26. Takamune, N., Kuroe, T., Tanada, N., Shoji, S. and Misumi, S. (2010) Biol Pharm Bull. **33**, 2018-2023
27. Shimozono, S. and Miyawaki, A. (2008) Methods Cell Biol. **85**, 381-393
28. Takamune, N., Gota, K., Misumi, S., Tanaka, K., Okinaka, S. and Shoji, S. (2008) Microbes Infect. **10**, 143-150
29. Lorenz, W. W., McCann, R. O., Longiaru, M. and Cormier, M. J. (1991) Proc Natl Acad Sci U S A. **88**, 4438-4442
30. Stein, I., Itin, A., Einat, P., Skaliter, R., Grossman, Z. and Keshet, E. (1998) Mol Cell Biol. **18**, 3112-3119
31. Greenberg, M. E., Bronson, S., Lock, M., Neumann, M., Pavlakis, G. N. and Skowronski, J. (1997) EMBO J. **16**, 6964-6976
32. Greenberg, M. E., Iafrate, A. J. and Skowronski, J. (1998) EMBO J. **17**, 2777-2789
33. Hartz, P. A., McMiller, T., Scott-Wright, D. and Samuel, K. P. (2003) Cell Mol Biol (Noisy-le-grand). **49**,

1101-1107
34. Cormack, B. P., Valdivia, R. H. and Falkow, S. (1996) Gene. **173**, 33-38
35. Yang, T. T., Cheng, L. and Kain, S. R. (1996) Nucleic Acids Res. **24**, 4592-4593
36. Bercovich, Z., Rosenberg-Hasson, Y., Ciechanover, A. and Kahana, C. (1989) J Biol Chem. **264**, 15949-15952
37. Cheng, Z., Garvin, D., Paguio, A., Stecha, P., Wood, K., Fan, F. (2010) Curr Chem Genomics. 4, 84-91
38. Morrison, T. B., Weis, J. J., Wittwer, C. T. (1998) Biotechniques **24**, 960-962
39. Hershko, A. and Ciechanover, A. (1998) Annu Rev Biochem. **67**, 425-479

Figure legends

Figure 1 Detection of heterogeneity of Nef expression levels. HEK293 cells transiently expressing each Nef using the pcDNA3.1 vector (A) or two clones of HEK293/CD4 cells expressing Nef_{NL4-3} or Nef_{JR-CSF} using the pcDNA4/HisMAX vector (B) were lysed and subjected to 5-20% SDS-PAGE, followed by western blot analysis using anti-V5 and anti-actin antibodies as described in Materials and Methods. The basic characteristics of the vector used in A and B are depicted in the bottom of the figure. The vector used in B has a translational enhancer sequence SP163 at upstream of the Nef coding region.

Figure 2 Immunostaining of Nef_{NL4-3} and Nef_{JR-CSF} expressed in HEK293/CD4 cells. The HEK293/CD4/Nef_{NL4-3} (top row) and HEK293/CD4/Nef_{JR-CSF} (bottom row) cells, which are stable Nef-expressing clonal cell lines, were immunostained using an anti-V5 antibody and an anti-mouse-FITC secondary antibody for Nef detection. The nucleus was stained with DAPI. The cells were observed using a Biozero digital microscope. Scale bar = 50 μm (rightmost panels).

Figure 3 Comparison of CD4 downregulation activities between Nef_{NL4-3} and Nef_{JR-CSF}. HEK293/CD4/Nef_{NL4-3} (top row panels) and HEK293/CD4/Nef_{JR-CSF} (bottom row panels) cells, which are stable Nef-expressing clonal cell lines, were stained with a PE-conjugated anti-CD4 antibody and then analyzed using a flow cytometer. HEK293/CD4 cells are depicted with the gray filled histogram, Nef-expressing HEK293/CD4 cells are depicted by the solid black line, and HEK293 cells are depicted in the striped histogram. Each MFI value is of the CD4 level in the cells expressing each Nef.

Figure 4 Induction of low expression property by AA129-206 of Nef_{NL4-3}

HEK293 cells were transiently transfected with each Nef, EGFP, or the Rluc fusion protein expression plasmid. The expression level of each Nef after 48-h transfection was analyzed by western blot analysis using an anti-V5 (B) or anti-Xpress antibody (D and E), as described in Materials and Methods. (A) Schematic representations of Nef_{NL4-3}, Nef_{JR-CSF}, and chimera Nef tested in "B". "B" shows a comparison of Nef_{NL4-3}, Nef_{JR-CSF}, and chimera Nef. (C) Schematic representations of EGFP, EGFP-NLAA129-206, and EGFP-CP tested in "D", EGFP, NLAA129-206-EGFP, and CP-EGFP tested in "E", and Rluc, NLAA129-206-Rluc, and CP-Rluc tested in "F". "D" shows a comparison of EGFP and AA129-206 or CP fusion to the *C*-terminal end of EGFP. "E" shows a comparison of EGFP and AA129-206 or CP fusion to the *N*-terminal end of EGFP. An asterisk marks an EGFP modified with unidentified posttranslational modification. "F" shows a comparison of Rluc and AA129-206 or CP fusion to the *N*-terminal end of Rluc. Rluc level was evaluated by measuring bioluminescent activity using coelenterazine h as the substrate, as described in Materials and Methods. Each bar represents the mean standard deviation (n = 3).

Figure 5 Comparison of low expression property of each deletion mutant.

(A) Schematic representations of NLAA129-206-EGFP or Rluc, NLAA142-206-EGFP or Rluc, NLAA129-186-EGFP or Rluc, and NLAA142-186-EGFP or Rluc tested in "A" or "B". HEK293 cells were transiently transfected with each EGFP or the Rluc fusion protein expression plasmid. The expression level of each fusion protein after 48-h transfection was analyzed by western blot analysis using an anti-Xpress antibody (B) or by measuring the bioluminescent activity of Rluc using coelenterazine h as the substrate (C) as described in Materials and Methods. Each bar represents the mean standard deviation (n = 3). Asterisks mark EGFPs modified with unidentified posttranslational modification (B).

Figure 6 Induction of low expression property by *C*-terminal region of Nef_{mac239} and Nef_{JR-CSF}.

(A) Schematic representations of EGFP or Rluc, CP-EGFP or CP-Rluc, macAA161-263-EGFP or macAA161-263-Rluc, and JRAA139-216-EGFP or JRAA139-216-Rluc tested in "B" or "C". HEK293 cells were transiently transfected with each expression plasmid of EGFP or Rluc and the CP, macAA161-263, and

JRAA139-216 fusion to the *N*-terminal end of EGFP or Rluc. The expression level of each fusion protein after 48-h transfection was analyzed by western blot analysis using an anti-Xpress antibody (B) or by measuring the bioluminescent activity of Rluc using coelenterazine h as the substrate (C), as described in Materials and Methods. Each bar represents the mean standard deviation (n = 3).

Figure 7 Quantification of mRNA levels by RT-qPCR
HEK293 cells were transfected with the Nef_{NL4-3}, Nef_{JR-CSF}, AA129-206-EGFP, CP-EGFP, or EGFP expression plasmid. Total RNA was extracted from these HEK293 cells and subjected to reverse transcription reaction, followed by qPCR using the Syber Green method. mRNA level was normalized to the transcript of the neomycin resistance gene, which is coded in the expression vector used. Each bar represents the mean standard deviation (n = 3). (A) Comparison of mRNA level between Nef_{NL4-3} and Nef_{JR-CSF}. (B) Comparison of mRNA level among AA129-206-EGFP, CP-EGFP, and EGFP

Figure 8 Effect of proteasome inhibitor on expression levels of Nef_{NL4-3} and AA129-206-EGFP
HEK293 cells expressing Nef_{NL4-3} (A) or AA129-206-EGFP (B) were treated with 20 μM MG132 for 0, 3, and 6 h. The expression levels of Nef_{NL4-3} and AA129-206-EGFP in HEK293 cells were analyzed by western blot analysis. The intensities of the bands were semiquantified with Fujifilm Image Gauge Software. The intensities of Nef_{NL4-3} and AA129-206-EGFP were normalized to that of actin. Each bar represents the mean standard deviation (n = 3).

Figure 1

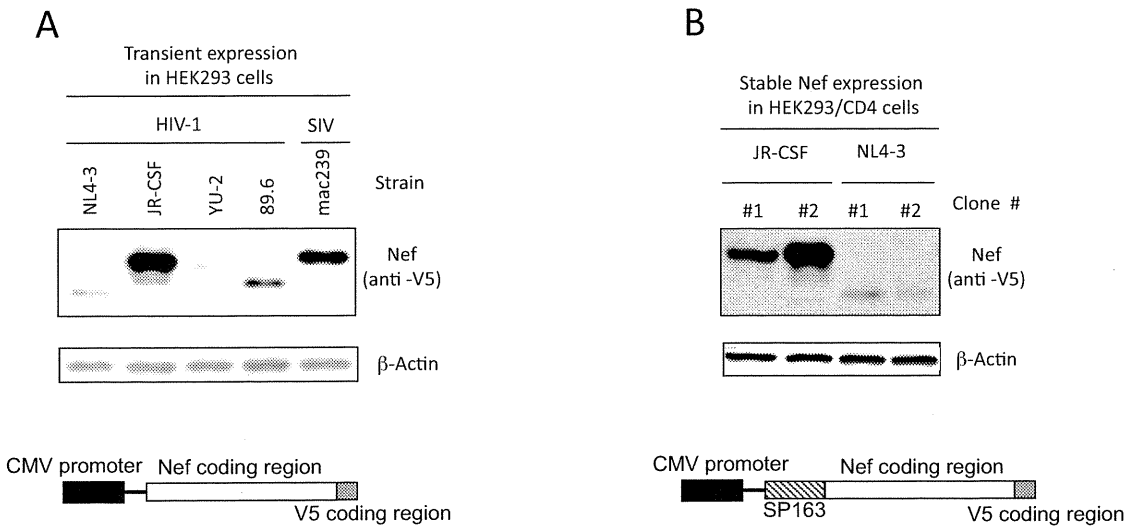

Figure 2

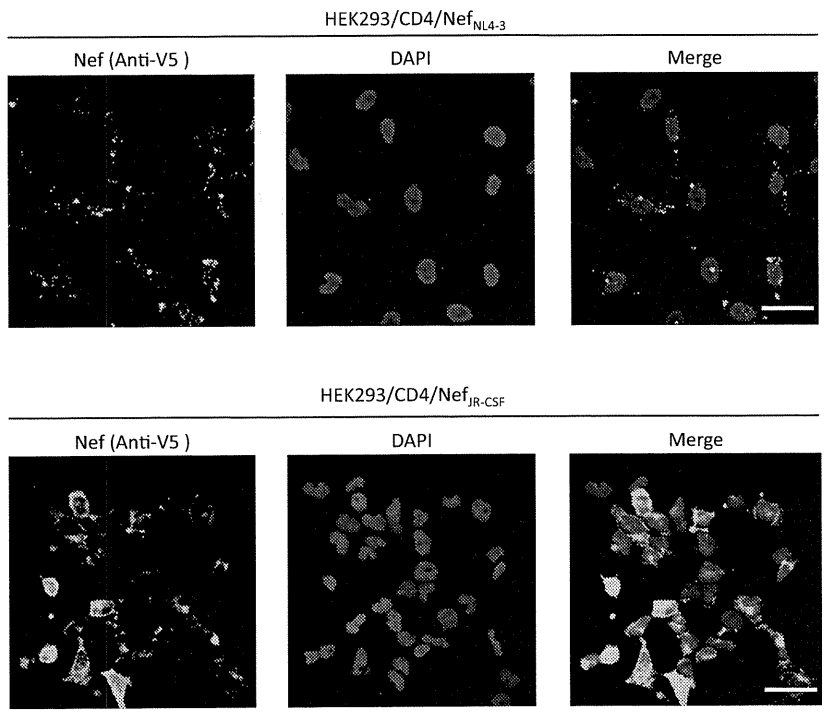

Figure 3

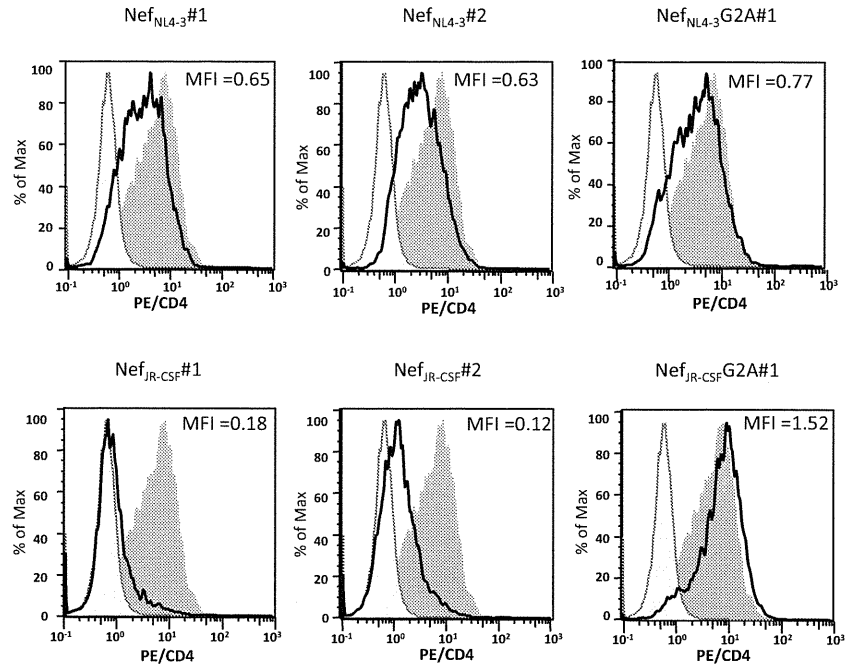

Figure 4

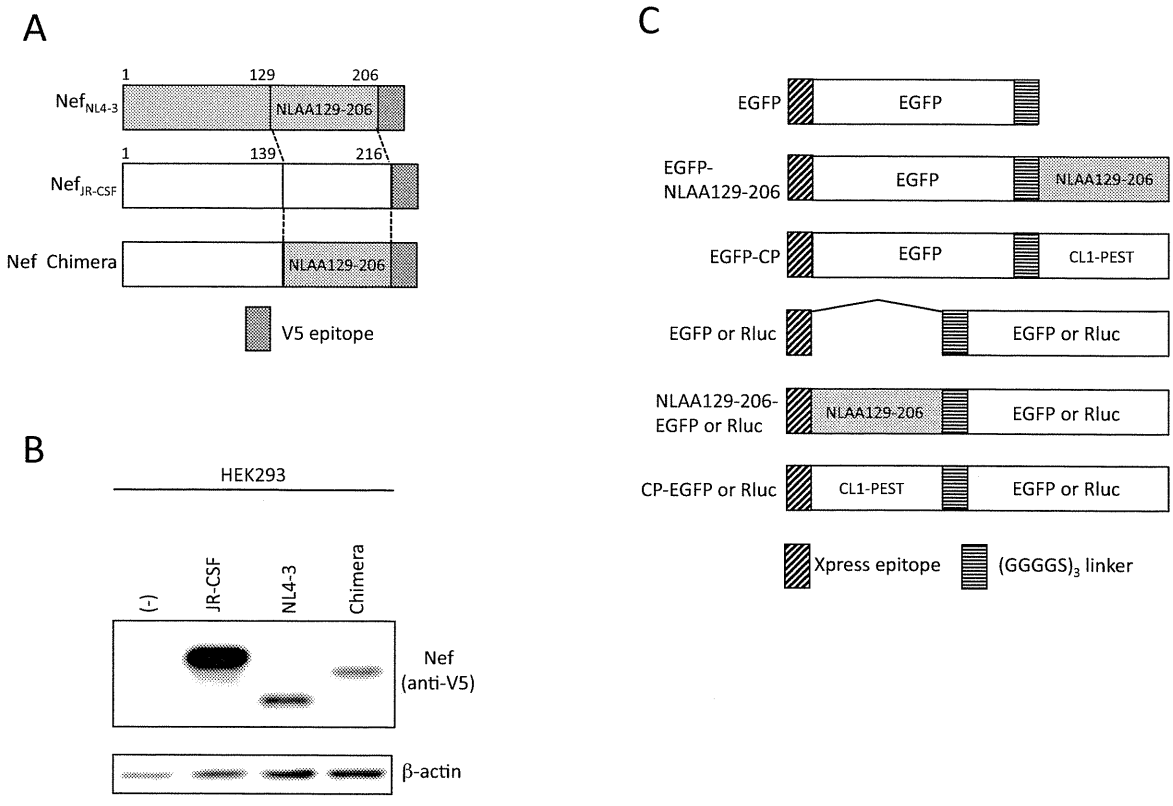

Figure 4

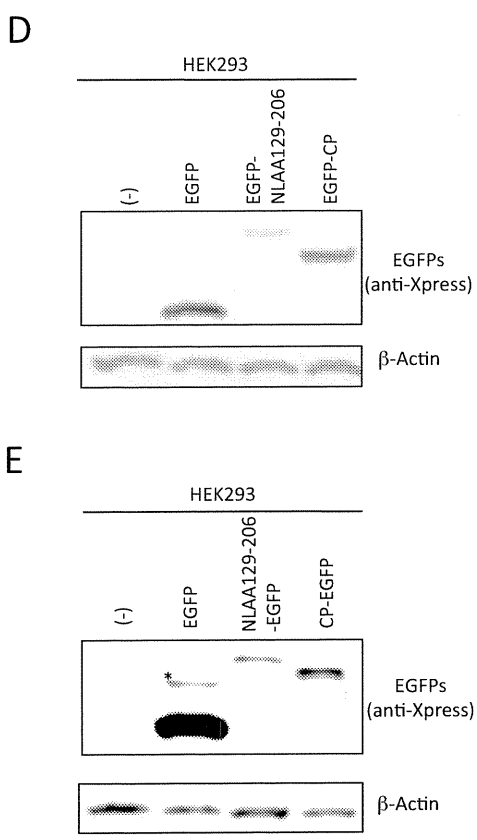

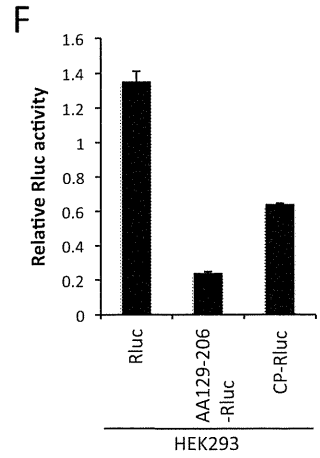

Figure 5

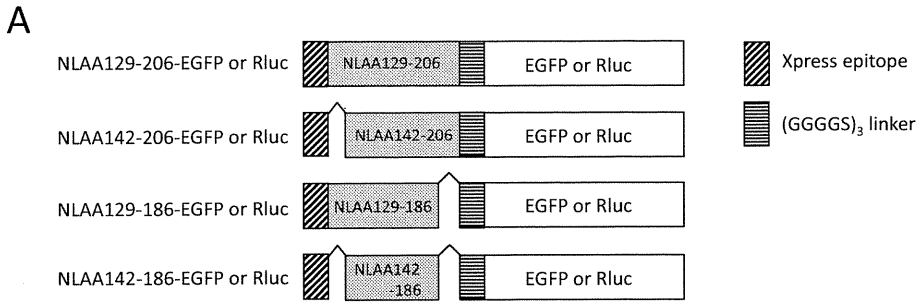

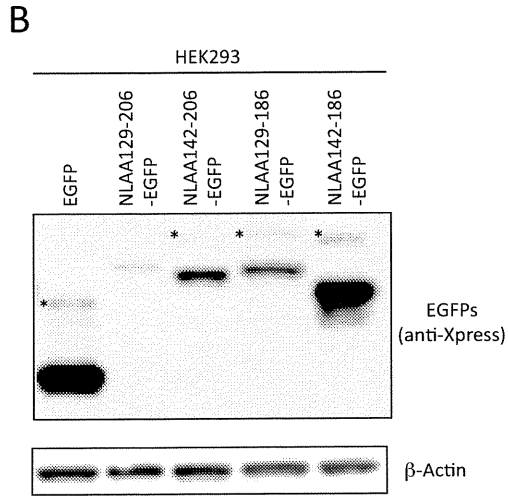

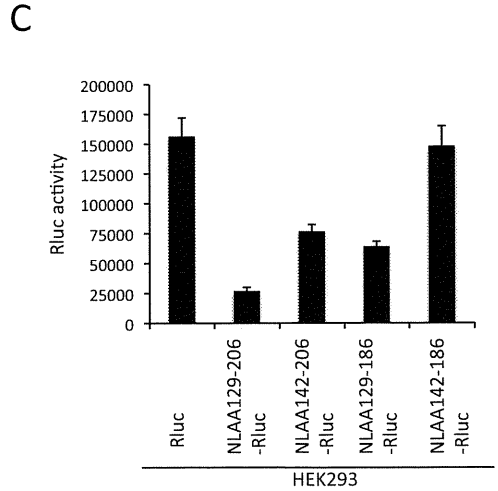

Figure 6

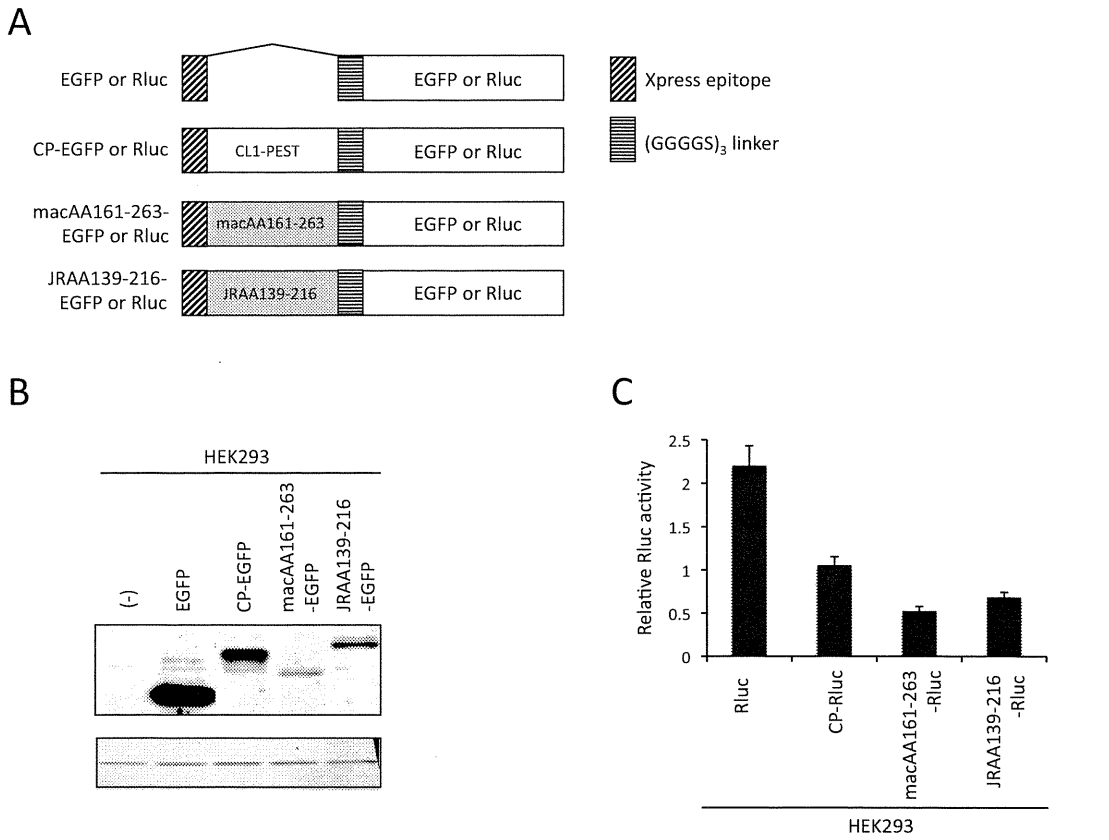

Figure 7

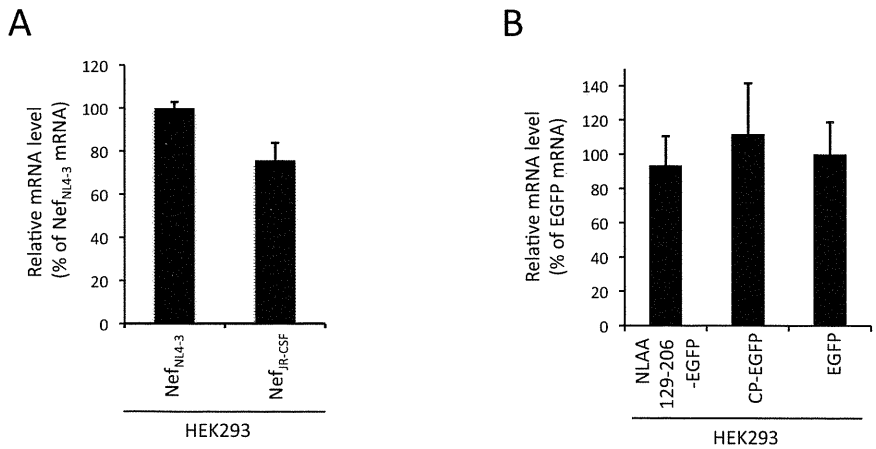

Figure 8

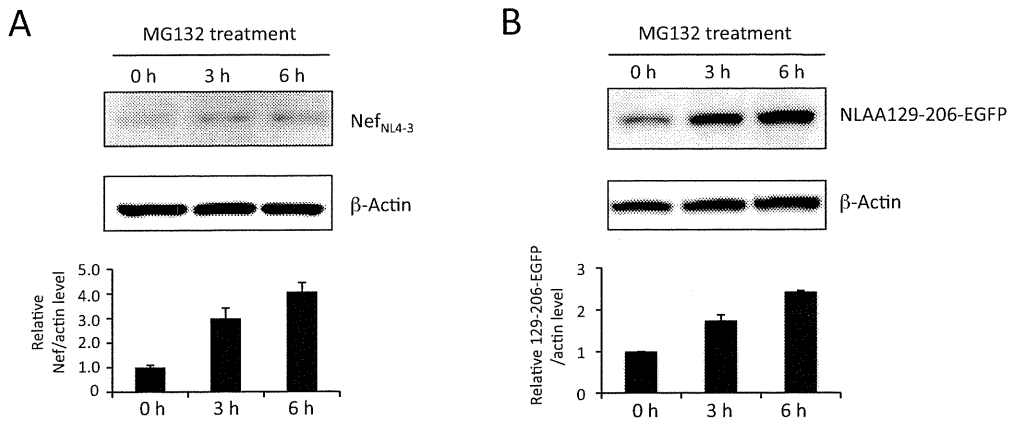
A
MG132 treatment
0 h
3 h
6 h
Nef$_{NL4-3}$
β-Actin
Relative Nef/actin level
5.0
4.0
3.0
2.0
1.0
0
0 h
3 h
6 h
B
MG132 treatment
0 h
3 h
6 h
NLAA129-206-EGFP
β-Actin
Relative 129-206-EGFP /actin level
3
2
1
0
0 h
3 h
6 h

Author's Choice

THE JOURNAL OF BIOLOGICAL CHEMISTRY VOL. 285, NO. 33, pp. 25185–25195, August 13, 2010

Uncoating of Human Immunodeficiency Virus Type 1 Requires Prolyl Isomerase Pin1*[S]

Received for publication, February 16, 2010, and in revised form, May 26, 2010 Published, JBC Papers in Press, June 7, 2010, DOI 10.1074/jbc.M110.114256

Shogo Misumi[‡1,2], Mutsumi Inoue[‡1,3], Takeo Dochi[‡], Naoki Kishimoto[‡], Naomi Hasegawa[‡], Nobutoki Takamune[‡], and Shozo Shoji[‡§]

From the [‡]Department of Pharmaceutical Biochemistry, Faculty of Medical and Pharmaceutical Sciences, Kumamoto University, Kumamoto 862-0973, Japan and [§]Kumamoto Health Science University, Kumamoto 861-5598, Japan

The process by which the human immunodeficiency virus type 1 (HIV-1) conical core dissociates is called uncoating, but not much is known about this process. Here, we show that the uncoating process requires the interaction of the capsid (CA) protein with the peptidyl-prolyl isomerase Pin1 that specifically recognizes the phosphorylated serine/threonine residue followed by proline. We found that the HIV-1 core is composed of some isoforms of the CA protein with different isoelectric points, and one isoform is preferentially phosphorylated in the Ser[16]-Pro[17] motif. The mutant virus S16A/P17A shows a severely attenuated HIV-1 replication and an impaired reverse transcription. The S16A/P17A change increased the amount of particulate CA cores in the cytosol of target cells and correlated with the restriction of HIV-1 infection. Glutathione *S*-transferase pulldown assays demonstrated a direct interaction between Pin1 and the HIV-1 core via the Ser[16]-Pro[17] motif. Suppression of Pin1 expression by RNA interference in a target cell results in an attenuated HIV-1 replication and increases the amount of particulate CA cores in the cytosol of target cells. Furthermore, heat-inactivated, inhibitor-treated, or W34A/K63A Pin1 causes an attenuated *in vitro* uncoating of the HIV-1 core. The Pin1-dependent uncoating is inhibited by antisera raised against a CA peptide phosphorylated at Ser[16] or treatment of the HIV-1 core with alkaline phosphatase. These findings provide insights into this obscure uncoating process in the HIV-1 life cycle and a new cellular target for HIV-1 drug development.

The HIV-1[4] CA protein must assemble properly and should be sufficiently stable to protect the genomic RNA but must disassemble to allow genomic RNA release after fusion. Because both the assembly and disassembly processes cannot act on the CA proteins at the same time, an important question concerns the mechanisms responsible for the switch from the assembly to disassembly mode. However, not much has been known about the disassembly process so far because this process has been assumed to occur immediately after fusion (1, 2).

Recent studies suggested that cell factors may assist the disassembly process, commonly referred to as uncoating (3, 4). Cellular activation has long been considered a requirement for HIV-1 infection of $CD4^+$ T cells, because HIV-1 fails to infect resting $CD4^+$ T cells from peripheral blood. Infection is aborted either during reverse transcription (5) or before nuclear import of the viral preintegration complex (6). It was shown that HIV-1 can enter resting $CD4^+$ T cells efficiently, but only short incomplete reverse transcripts are formed. Auewarakul *et al.* (3) demonstrated that the uncoating of HIV-1 is efficiently induced by lysate from activated $CD4^+$ lymphocytes, whereas resting $CD4^+$ lymphocyte lysate cannot uncoat the HIV-1 core. Furthermore, Warrilow *et al.* (4) reported that endogenous reverse transcription is inefficient in comparison with reverse transcription in cell infection, as exemplified by the poor efficiency of the production of intravirion late reverse transcription products. This observation also suggests a requirement for a contribution from the host cell environment for optimal HIV-1 reverse transcription to proceed by an ordered disassembly of the HIV-1 CA core. These findings suggest that the uncoating activity that releases the CA protein from the HIV-1 core is due to cellular factors.

We previously reported that the HIV-1 core is composed of some isoforms of the CA protein with different isoelectric points (7). The difference in isoelectric points among CA protein isoforms might be due to multiple post-translational modifications, such as phosphorylation. Indeed, several reports have provided evidence that the CA protein is predominantly phosphorylated at serine residues rather than threonine/tyrosine residues (8, 9). Phosphorylation often plays an important role in modulating protein activity and protein-protein interactions and promoting the disassembly of cellular macromolecular assembly such as the nuclear pore complex. Protein kinases catalyze post-translational phosphorylation, and many kinases are themselves regulated by phosphorylation. The phosphor-

* This work was supported in part by a Grant-in-Aid for Scientific Research from the Ministry of Education, Culture, Sports, Science, and Technology of Japan and a Health Science Research Grant from the Ministry of Health, Labour, and Welfare of Japan.

Author's Choice—Final version full access.

[S] The on-line version of this article (available at http://www.jbc.org) contains supplemental Table S1 and Figs. S1–S5.

[1] Both authors contributed equally to this work.

[2] To whom correspondence should be addressed: Kumamoto University, Dept. of Pharmaceutical Biochemistry, Faculty of Medical and Pharmaceutical Sciences, 5-1 Oe-Honmachi, Kumamoto 862-0973, Japan. Tel.: 81-96-371-4362; Fax: 81-96-362-7800; E-mail: misumi@gpo.kumamoto-u.ac.jp.

[3] Recipient of Japan Society for the Promotion of Science for Young Scientists Research Fellowship 217212.

[4] The abbreviations used are: HIV-1, human immunodeficiency virus type 1; CA, capsid; GST, glutathione *S*-transferase; CPE, cytopathic effect; ALP, alkaline phosphatase; RT, reverse transcriptase; PBS, phosphate-buffered saline; CBB, Coomassie Brilliant Blue; MALDI-TOF, matrix-assisted laser desorption ionization time-of-flight; KLH, keyhole limpet hemocyanin; ELISA, enzyme-linked immunosorbent assay; WT, wild type; mAb, monoclonal antibody; siRNA, small interfering RNA; RPDE, relative percentage of disassembly efficiency; MA, matrix; SIV, simian immunodeficiency virus.

ylation-dependent modulation of protein-protein interactions is the pivotal molecular switch for the regulation of signaling processes within eukaryotic cells. Furthermore, current studies point toward mitotic phosphorylation of nucleoporins as the trigger of the nuclear pore complex disassembly process (10–12). These findings led to a hypothesis that phosphorylation induces the dissociation of CA-CA protein interactions and promotes the disassembly of the HIV-1 core.

In this study, we show that the serine residue in the Ser^{16}-Pro^{17} motif of a CA protein isoform is phosphorylated and that peptidyl-prolyl isomerase Pin1 specifically recognizes the Ser^{16}-Pro^{17} motif of the HIV-1 core. Furthermore, we demonstrated that Pin1 prolyl isomerase activity is required for the disassembly of the HIV-1 core. These results reveal a novel regulation step of HIV-1 infection.

EXPERIMENTAL PROCEDURES

Virus Preparation—HIV-1_{LAV-1} and HIV-1_{JRFL} were prepared as previously described (7, 13). The supernatant from the culture medium of CEM/LAV-1 or CEM-CCR5/JRFL was filtered through a 0.22-μm-pore size disposable filter and then centrifuged at 43,000 × *g* for 3 h at 4 °C. The obtained pellet was resuspended in PBS(−) (0.02% KH_2PO_4, 0.29% $Na_2HPO_4{\cdot}12H_2O$, 0.8% NaCl, 0.02% KCl) and then centrifuged at 100,000 × *g* for 1 h at 4 °C. The resulting pellet was resuspended in 10 mM Tris-HCl buffer (pH 8.0). Virions were treated with or without 1 mg/ml subtilisin (ICN Biomedicals Inc., Costa Mesa, CA) in 10 mM Tris-HCl (pH 8.0) and 1 mM EDTA-2Na. The virions were then purified using PBS(−) by column chromatography with a 10-ml column of Sepharose CL-4B™ at room temperature in a biosafety hood. Fractions containing the virus were pooled and centrifuged at 100,000 × *g* for 1 h at 4 °C. The resulting pellet derived from HIV-1_{LAV-1} or HIV-1_{JRFL} was boiled for 1 min and lysed in 200 μl of lysis buffer (9.5 M urea, 2% (w/v) Nonidet P-40, 2% ampholine (pH 6–8), and 5% 2-mercaptoethanol). For the MAGIC-5 assay and quantitative analysis of HIV-1 reverse transcription, pNL4-3-based mutants and replication-defective viruses were prepared as follows. The HIV-1 proviral DNA constructs pNL4-3 (14), containing full-length HIV-1, and pNL4-3Δenv, in which there is a truncation in *env*, were the control viruses utilized in this study. The 1136-bp fragment containing the BssHII and SpeI sites of pNL4-3 or pNL4-3Δenv was subcloned into pT7Blue (Novagen, Inc., Madison, WI). Point mutations were introduced into the Ser^{16}-Pro^{17} motif in the HIV_{NL4-3} or $HIV_{NL4-3\Delta env}$ CA protein by site-directed mutagenesis. The fragments were sequenced to confirm mutations. The mutant BssHII-SpeI fragment was recloned into the full-length HIV expression plasmid $pNL4\text{-}3_{BssHII\text{-}SpeI}$ or $pNL4\text{-}3\Delta env_{BssHII\text{-}SpeI}$, which does not have the backbone BssHII-SpeI fragment. All of the mutations were verified by sequencing. The mutant viruses ($HIV_{NL4-3(S16A/P17A)}$, $HIV_{NL4-3\Delta envWT}$, and $HIV_{NL4-3\Delta env(S16A/P17A)}$) were produced by the transient transfection of HEK293 cells using pNL4-3(S16A/P17A) or pNL4-3Δenv and pNL4-3Δenv(S16A/P17A) with the pNL4-3-based env expression vector. Four days after transfection, the virus-containing supernatant was collected and clarified by filtration through 0.45-μm-pore size filters. Virus production and release were monitored by measuring virion-associated RT activity as previously described (7).

Peptide Mass Fingerprinting—An aliquot of the viral lysate was subjected to two-dimensional polyacrylamide gel electrophoresis in accordance with the method of O'Farrell (15). The sample was loaded using a 15-cm immobilized pH gradient tube gel (pH 6–8) (Daiichi Pure Chemicals Co., Ltd.). The proteins were focused for 1 h at 400 V followed by a step gradient (1000 V for 18 h; 2000 V for 1 h). After the second-dimensional run (10–20% PAG large gel; Daiichi Pure Chemicals Co., Ltd.), the gel was stained with Coomassie Brilliant Blue (CBB) R-250 or ProQ diamond (Invitrogen). CBB-stained gel pieces were excised from the gel and immersed in 100 μl of acetonitrile, dried under vacuum centrifugation, rehydrated in 25 μl of trypsin solution (3.9 ng/μl trypsin in 170 mM ammonium bicarbonate, 40% $H_2{}^{18}O$, 30% acetonitrile) or 25 μl of Glu-C solution (10 ng/μl Glu-C in 55 mM NaH_2PO_4 and 40% $H_2{}^{18}O$), and then incubated for 60 min. The unabsorbed enzyme solution was removed, and the gel pieces were incubated for 12 h at 37 °C. The digested peptides were purified using ZipTip (Nihon Millipore Ltd., Tokyo, Japan) and then analyzed by MALDI-TOF mass spectrometry as previously described (7). Phosphorylated peptides were analyzed as follows. Alkaline phosphatase (Wako Pure Chemical Industries, Ltd.) liberated the phosphate group from phosphorylated peptides. Alkaline phosphatase reactions were carried out directly on the MALDI target. The sample was mixed with 12 ng/ml ALP from *Escherichia coli* (Wako Pure Chemical Industries) that had been dissolved in 10 mM ammonium bicarbonate. The reactions were carried out for 5 min at room temperature followed by the addition of 0.5 μl of α-cyano-4-cinnamic acid or 2,5-dihydroxybenzoic acid saturated in 40% acetonitrile, 0.1% trifluoroacetic acid.

Preparation of HIV-1 p24-derived Peptide-Keyhole Limpet Hemocyanin (KLH) Conjugates and Antibody Screening—A p24-derived linear decapeptide (pSP, H_2N-HQAIpSPRTLN-COOH) was synthesized using an automatic peptide synthesizer. The molecular mass was determined by MALDI-TOF mass spectrometry (Burker Franzen Analytik). The amino group of His^1 was coupled to KLH (pSP-KLH) through bis(sulfosuccinimidyl)suberate (Thermo Fisher Scientific Inc.). Ten BALB/c mice were immunized intraperitoneally with 200 μg of pSP-KLH in Freund's adjuvant at 1-week intervals and administered an intravenous boost of 40 μg of pSP-KLH 3 days prior to splenectomy. The blood samples were collected prior to euthanasia and centrifuged at 1500 × *g* for 5 min, and the anti-pS16/P17 serum was harvested. Then the mice were euthanized, and their spleens were removed for *in vitro* hybridoma cell production. The hybridomas were generated by a standard method, by which splenocytes were fused with P3U1 cells and selected in hypoxanthine-, aminopterin-, and thymidine-supplemented media. In the screening, supernatants were tested for reactivity to ELISA plates coated with pSP. The hybridoma that produced high titers of anti-pS16/P17 mAb (3/D-6) was then cloned.

Preparation of HIV-1 CA Cores and Detection of Phosphorylated CA Protein in the HIV Core—The WT HIV CA cores were purified in accordance with the method of Auewarakul *et al.* (3) with some modifications. Briefly, 3 ml of purified cell-free viruses was overlayered on a discontinuous sucrose density gra-

dient. The gradient was composed of 1 ml of 50% sucrose at the bottom and 1 ml of 10% sucrose containing 0.1% Igepal CA-630 on the top. The overlayered gradient was then centrifuged at 100,000 × *g* in a Swing Rotor P65ST (HitachiKoki Co., Ltd.) for 2 h at 4 °C. The pellets containing viral cores were then resuspended in the uncoating assay buffer (50 mM NaH_2PO_4, pH 7.2, 150 mM NaCl, and 200 μM sodium orthovanadate) and pooled. The CA cores were quantitated by measuring HIV-1 p24 antigen with RETRO-TEK HIV-1 p24 antigen ELISA (ZeptoMetrix Corp.). To examine the Ser^{16} phosphorylation of CA core, the pellets containing viral cores were then lysed with 62.5 mM Tris-HCl, 2% SDS, 10% glycerol (pH 6.8), and 10% 2-mercaptoethanol. The lysate from HIV cores was subjected to SDS-PAGE, and separated products were transferred to a polyvinylidene difluoride membrane for Western blotting. The membrane was stained with normal mouse serum and anti-pS16/P17 serum raised against pSP-KLH with or without pSP.

Viral Infectivity Assay—Jurkat and CEM cells (1 × 10^5) were exposed to the HEK293 cell-derived WT virus or S16A/P17A variant (100 ng of p24 antigen) for 2 h at 37 °C, washed with PBS(−), and cultured for 96 h. Virus infectivity was monitored by measurement of the p24 antigen from cell culture supernatants using RETRO-TEK HIV-1 p24 antigen ELISA (ZeptoMetrix Corp.).

Viral Entry Assay and Quantitative Analysis of HIV-1 Reverse Transcription during Acute Infection—The entry level of WT or mutant viruses was determined as follow. Viral entry assay was performed using the protocol of Kawano *et al.* (16) with modifications. MAGIC-5 cells (1 × 10^6 cells) were exposed to the virus (213.9 ng of HIV-1 RT) at 37 °C for 2 h. The cells were washed with PBS(−) and then incubated for 5 min at 37 °C in PBS(−) containing 0.25% trypsin. After trypsinization, the cells were washed twice with PBS(−) and pelleted. Cell-associated CA antigen content was determined by Western immunoblot analysis using an anti-p24 mAb (Immuno Diagnostics, Inc.). Furthermore, *de novo* synthesized HIV-1 cDNA was analyzed with or without Pin1 siRNA treatment in accordance with the method of Ikeda *et al.* (17).

Electron Microscopy of Virus—A viral preparation was fixed with 0.1 M sodium phosphate buffer (pH 7.4) containing 2% paraformaldehyde and 2.5% glutaraldehyde at 4 °C for 2 h prior to postfixation with 1% osmium tetroxide for 30 min at 4 °C. After dehydration in ethanol, the specimens were embedded in epoxy resin.

MAGIC-5 Assay and Cytopathic Effect (CPE) Assay—Viral infectivity was determined using MAGIC-5 cells as previously described in Ref. 18. MAGIC-5 cells (1 × 10^4 cells) were incubated in suspensions of WT, mutant, or single-round replication-defective viruses with 20 μg/ml DEAE dextran for 2 h and then cultured in a medium (200 μl) for 48 h. The cells were fixed, and HIV-1-infected cells identified by their blue staining were counted by conventional methods. To further examine whether a decrease in endogenous Pin1 expression level decreases viral infectivity, both MAGIC-5 assay and CPE assay were performed. 60 nM small interfering RNA against Pin1 (Pin1 C1 sense siRNA, GCCAUUUGAAGACGCCUCGdTdT; Pin1 C1 antisense siRNA, GAGGCGUCUUCAAAUGGCdTdT; Pin1 C2 sense siRNA, CUGGCCUCACAGUUCAGCGdTdT; Pin1 C2 antisense siRNA, CGCUGAACUGUGAGGCCAGdTdT; Pin1 C3 sense siRNA, GCCGAGUGUACUACUUCAAdTdT; or Pin1 C3 antisense siRNA, UUGAAGUAGUACACUCGGCdTdT) or control siRNA (sense siRNA against GL2 Luciferase, CGUACGCGGAAUACUUCGAdTdT; or antisense siRNA, UCGAAGUAUUCCGCGUACGdTdT) was transfected into the MAGIC-5 cells (1 × 10^4 or 2 × 10^5 cells) using Lipofectamine 2000. The cells were infected with HIV-1_{LAV-1} (12 ng of p24 antigen). HIV-1_{LAV-1}-infected cells identified by their blue staining were counted by conventional methods. In CPE assay, the cells were infected with a single-round replication-defective HIV-1 ($HIV_{NL4-3\Delta envWT}$, 11 ng of HIV RT).

Fate-of-Capsid Assay—Fate-of-capsid assay was performed in accordance with the method of Sodroski and co-workers (19) with some modifications. Briefly, recombinant HIV-1 virus-like particles (WT HIV-1(VSV-G) and S16A/P17A HIV-1(VSV-G)) were produced by cotransfection of 293T cells with pHCMV-G and pNL4-3Δenv or pNL4-3Δenv carrying the S16A/P17A mutation (pNL4-3Δenv(S16A/P17A)) as described in Ref. 20. To examine whether the infectivity defect of the S16A/P17A variant is linked to a dysfunction of uncoating, MAGIC-5 (4.5 × 10^6) cells were seeded in 60-cm^2 flasks and the next day incubated with either 5 ml of WT HIV-1(VSV-G) or 5 ml of S16A/P17A HIV-1(VSV-G) incubated at 37 °C for 4 h after 30 min of incubation at 4 °C. On the other hand, to examine whether Pin1 depletion is linked to a dysfunction of uncoating, MAGIC-5 cells (4.0 × 10^6) were transfected with Pin1 C1 and C2 siRNA (600 nM) or control siRNA (600 nM) using Neon™ transfection system (Invitrogen) and incubated for 44 h. The cells were further incubated with 5 ml of WT HIV-1(VSV-G) at 37 °C for 4 h after 30 min of incubation at 4 °C. These cells were washed three times with ice-cold PBS and detached by incubating with 2 ml of proteinase K (7 mg/ml in Dulbecco's modified Eagle's medium) for 5 min at 4 °C. The cells were washed once in Dulbecco's modified Eagle's medium containing 10% fetal bovine serum and twice in PBS. The pellets were resuspended in 2 ml of hypotonic lysis buffer (10 mM Tris-HCl, pH 8.0, 10 mM KCl, and 1 mM EDTA) and placed on ice for 15 min. The cells were lysed using a 7-ml Dounce homogenizer and 15 strokes with pestle B. Cell debris was removed by centrifugation for 3 min at 2,000 × *g*. After centrifugation, 1 ml of lysate was layered onto a 3.5-ml of 50% sucrose cushion (made in PBS) and centrifuged at 125,000 × *g* for 2 h at 4 °C in a Swing Rotor P65ST (HitachiKoki Co., Ltd). After centrifugation, 150 μl from the topmost part of the supernatant was collected and made 1× in SDS sample buffer. The pellets were resuspended in 10 μl of 1× SDS sample buffer. The samples were subjected to SDS-PAGE and Western blotting for CA proteins.

Determination of Pin1-CA Interaction—The interaction between Pin1 and the CA core was determined by GST-Pin1 pulldown assay. Recombinant Pin1 proteins were produced as N-terminal GST-tagged proteins as previously described (21). The CA core was treated with ALP (Wako Pure Chemical Industries) or heat-denatured ALP for 2 h (final concentration, 0.024 μg/μl ALP) in a buffer containing 50 mM NaH_2PO_4 (pH 7.2), 150 mM NaCl, 200 μM sodium orthovanadate, 10% glycerol, and 1% Triton X-100 and then incubated with 30 μl of beads containing GST or GST-Pin1 proteins for 2 h at 4 °C.

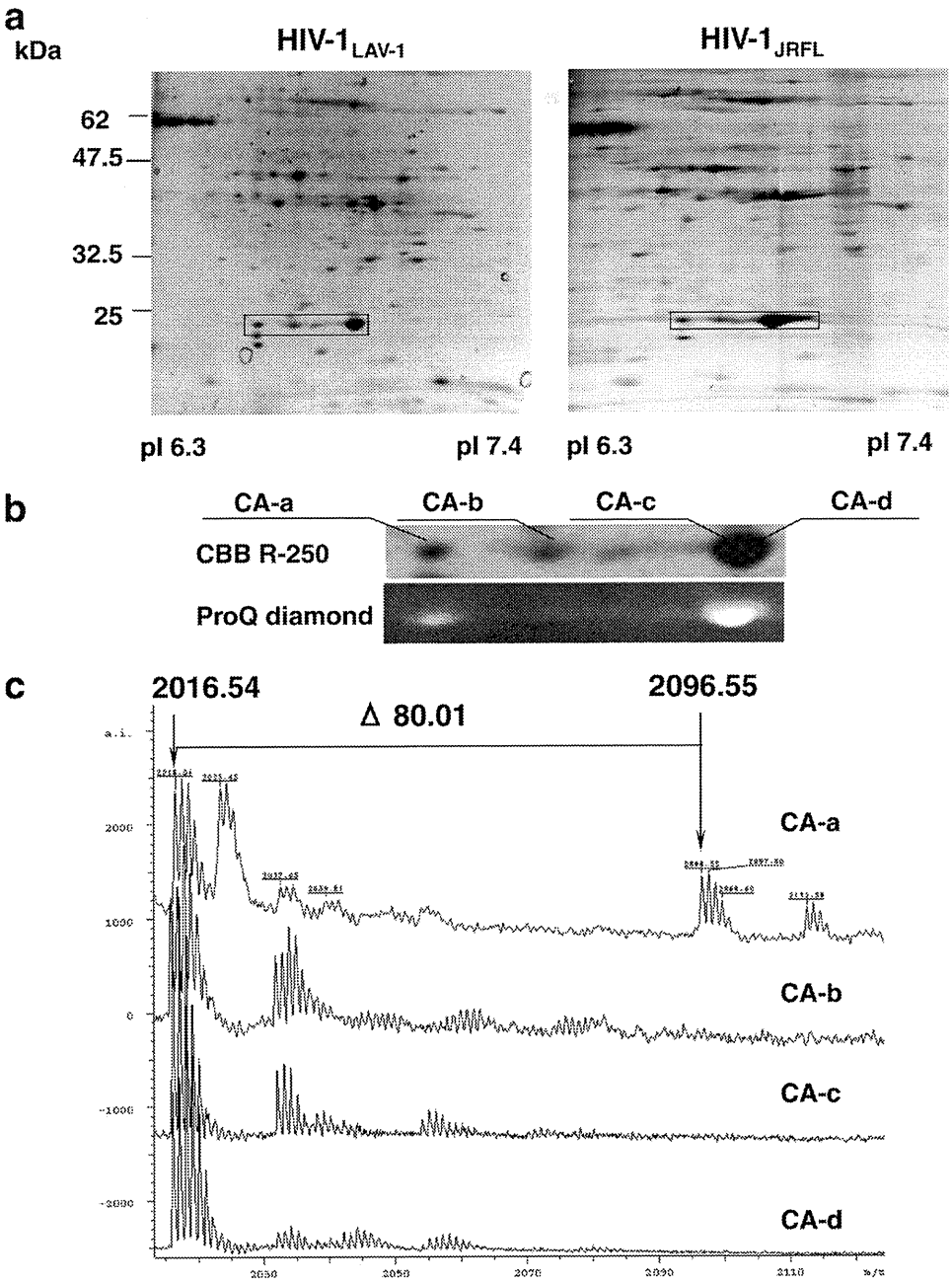

FIGURE 1. **A serine residue in the Ser[16]-Pro[17] motif of a CA isoform is selectively phosphorylated.** *a*, CBB R-250-stained two-dimensional gel images of HIV-1_{LAV-1} and HIV-1_{JRFL}. The *rectangles* indicate CA isoforms in virions. *b*, CBB R-250 and ProQ diamond staining of CA isoforms of HIV-1_{LAV-1}. *c*, spectra of *N*-terminal tryptic peptides derived from CA isoforms of HIV-1_{LAV-1}. The peak of $[M+H]^+$ at *m/z* 2096.55 corresponds to the phosphorylated form of the N-terminal tryptic peptide Pro_1-Arg_{18} of CA-a. *d*, liberation of phosphate group from N-terminal phosphorylated Pro_1-Arg_{18} derived from CA-a using alkaline phosphatase. The *lower* and *upper panels* show samples treated and not treated with alkaline phosphatase, respectively. The phosphorylated Pro_1-Arg_{18} disappeared after the phosphatase treatment. *e*, incorporation of phosphorylated CA-a into HIV core. The purified HIV core is subjected to Western immunoblot analysis using normal sera or anti-pS16/P17 serum with or without pSP, H_2N-HQAIpSPRTLN-COOH.

Immunoblotting analysis was performed using an anti-p24 mAb (Immuno Diagnostics, Inc.). Furthermore. a fraction of the ALP-treated CA core was subjected to Western blot analysis using an anti-pS16/P17 mAb raised against a synthetic phosphoserine-containing peptide, pSP, or an anti-p24 mAb.

Suppression of Pin1 Expression by siRNA—MAGIC-5 cells were transfected with Pin1 C3 siRNA (30–120 nM) or control siRNA (30–120 nM). The cells were infected with the WT virus and harvested 2 h after infection. To confirm the level of Pin1 expression, immunoblot analysis was carried out using the chemiluminescence protocol. The mouse monoclonal and goat polyclonal antibodies used were as follows: anti-Pin1 (R & D Systems, Inc.), anti-actin (Oncogene™ research product), and anti-lactate dehydrogenase (Chemicon) antibodies.

Uncoating Assay—The WT HIV CA core was purified as described above. The purified CA cores (2 ng) were resuspended in the uncoating assay buffer (50 mM NaH_2PO_4, pH 7.2, 150 mM NaCl, 200 μM sodium orthovanadate) and incubated with 0.114 μg/μl GST-Pin1, 0.114 μg/μl heat-denatured GST-Pin1, 0.114 μg/μl GST-Pin1 treated with juglone (molar ratio of GST-Pin1:juglone = 1:10; juglone was preincubated with GST-Pin1 at 37 °C for 1 h and then removed by gel filtration) or 0.114 μg/μl GST-Pin1(W34A/K63A) at 37 °C for 1 h. To examine whether the extent of CA disassembly was enhanced by Pin1, the pellets from the uncoating reactions were subjected to Western blot analysis using the anti-p24 mAb. Furthermore, a fraction of purified CA cores was pretreated with anti-pS16/P17 sera or normal sera. Another fraction of purified CA cores was treated with ALP (final concentration, 0.345 μg/μl) or heat-denatured ALP (final concentration, 0.345 μg/μl). The resulting CA cores were incubated with 0.114 μg/μl GST-Pin1 at 37 °C for 1 h. Each core suspension was then diluted in 5 ml of uncoating assay buffer and centrifuged at 100,000 × *g* for 2 h at 4 °C. The extent of CA release is quantified by p24 ELISA (ZeptoMetrix Corporation; the detection limit for the p24 antigen by ELISA was 7.8 pg/ml as provided by the manufacturer) because the undissociated cores were pelleted, and the dissociated CA protein was in the supernatant after ultracentrifugation. The relative percentage of disassembly efficiency (RPDE) is given by RPDE (%) = 100 × $(CA_S/CA_T)/(CA_{SC}/CA_{TC})$, where CA_S is the concentration of the CA protein in the supernatant, CA_T is the concentration of total CA protein in the supernatant plus pellet in the disassembly experiments of the CA core using boiled, juglone-treated

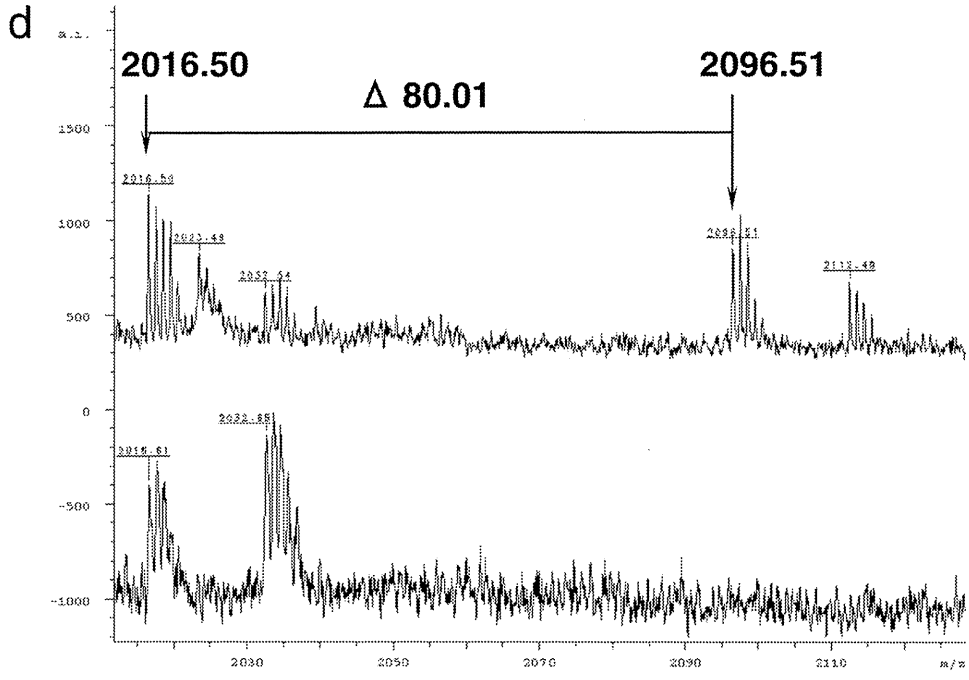

FIGURE 1—*continued*

GST-Pin1, or GST-Pin1(W34A/K63A); CA_{SC} is the concentration of the CA protein in the supernatant; and CA_{TC} is the concentration of total CA protein in the supernatant plus pellet in the control experiment using GST-Pin1. Likewise, the RPDE of CA cores pretreated with anti-pS16/P17 sera or ALP is given by RPDE (%) = $100 \times (CA_S/CA_T)/(CA_{SC}/CA_{TC})$, where CA_S is the concentration of CA protein in the supernatant; CA_T is the concentration of total CA protein in the supernatant plus pellet in the disassembly experiments of CA core pretreated with anti-pS16/P17 sera or ALP using the GST-Pin1; CA_{SC} is the concentration of CA protein in the supernatant; and CA_{TC} is the concentration of total CA protein in the supernatant plus pellet in the control experiments of CA core pretreated with normal mouse sera or heat-denatured ALP using the GST-Pin1.

RESULTS

A CA Protein Isoform Is Selectively Phosphorylated at Serine Residue 16 in the Ser[16]-Pro[17] Motif and Incorporated into the HIV Core—Some isoforms of the HIV-1 CA protein associated with CXCR4-tropic HIV-1_{LAV-1} or CCR5-tropic HIV-1_{JRFL} were identified by proteomics using two-dimensional gel electrophoresis and MALDI-TOF mass spectrometry (Fig. 1*a* and supplemental Table S1). We found that four isoforms of the HIV-1_{LAV-1} CA protein (CA-a (pI 6.70), CA-b (pI 6.80), CA-c (pI 6.91), and CA-d (pI 6.95)) are inside the virion (Fig. 1*b*). The differences between the pI values of the four isoforms of the CA protein may be due to post-translational modifications, such as phosphorylation and formylation (8, 9, 22, 23). Indeed, the CA proteins are composed of phosphorylated and unphosphorylated (Fig. 1*b*, *lower panel*) and formylated isoforms (23). Peptide mass fingerprinting data were used to identify the probable co/post-translational modifications. Then the specific phosphorylation of the N-terminal tryptic peptide ([1]PIVQNIQGQMVHQAISPR[18]) of CA-a was estimated because the spectrum corresponding to the N-terminal tryptic peptide exhibited a peak at *m/z* 2016.54 and the mass spectrum corresponding to the phosphorylated form exhibited a peak at *m/z* 2096.55 (Fig. 1*c*). The phosphorylation was confirmed by the liberation of a phosphate group from the N-terminal peptide of CA-a. The peak of $[M+H]^+$ at *m/z* 2016.50 corresponded to the peptide ([1]PIVQNIQGQMVHQAISPR[18]) whose phosphate group was cleaved off by an alkaline phosphatase (ALP) (Fig. 1*d*). These results show that the serine residue in the Ser^{16}-Pro^{17} motif of CA-a is selectively phosphorylated. To further determine whether CA-a is actually present in the CA core, the WT CA core was purified in accordance with the method of Auewarakul *et al.* (3) and was subjected to Western blot analysis using anti-pS16/P17 serum with or without pSP. As shown in Fig. 1*e*, CA-a is actually incorporated into the CA core.

Mutation at the Ser[16]-Pro[17] Motif Affects Uncoating Process—To study the role of the phosphorylated Ser^{16} that precedes Pro, we replaced Ser^{16} with glutamic acid (S16E) or alanine (S16A) to mimic phosphorylated or unphosphorylated Ser, respectively. We then tested the infectivity of the mutants by MAGIC-5 assay (21). The results showed that the S16E variant had the same infectivity as the wild type (Fig. 2*a*, *WT*). In contrast, the S16A variant had a decreased infectivity (Fig. 2*a*, $p < 0.01$). Assuming that glutamic acid mimics the negative charge of phosphorylated Ser^{16} in only a fraction of the CA protein in a viral core, the results obtained for S16E or S16A suggest that phosphorylation at Ser^{16} plays a critical role in maintaining

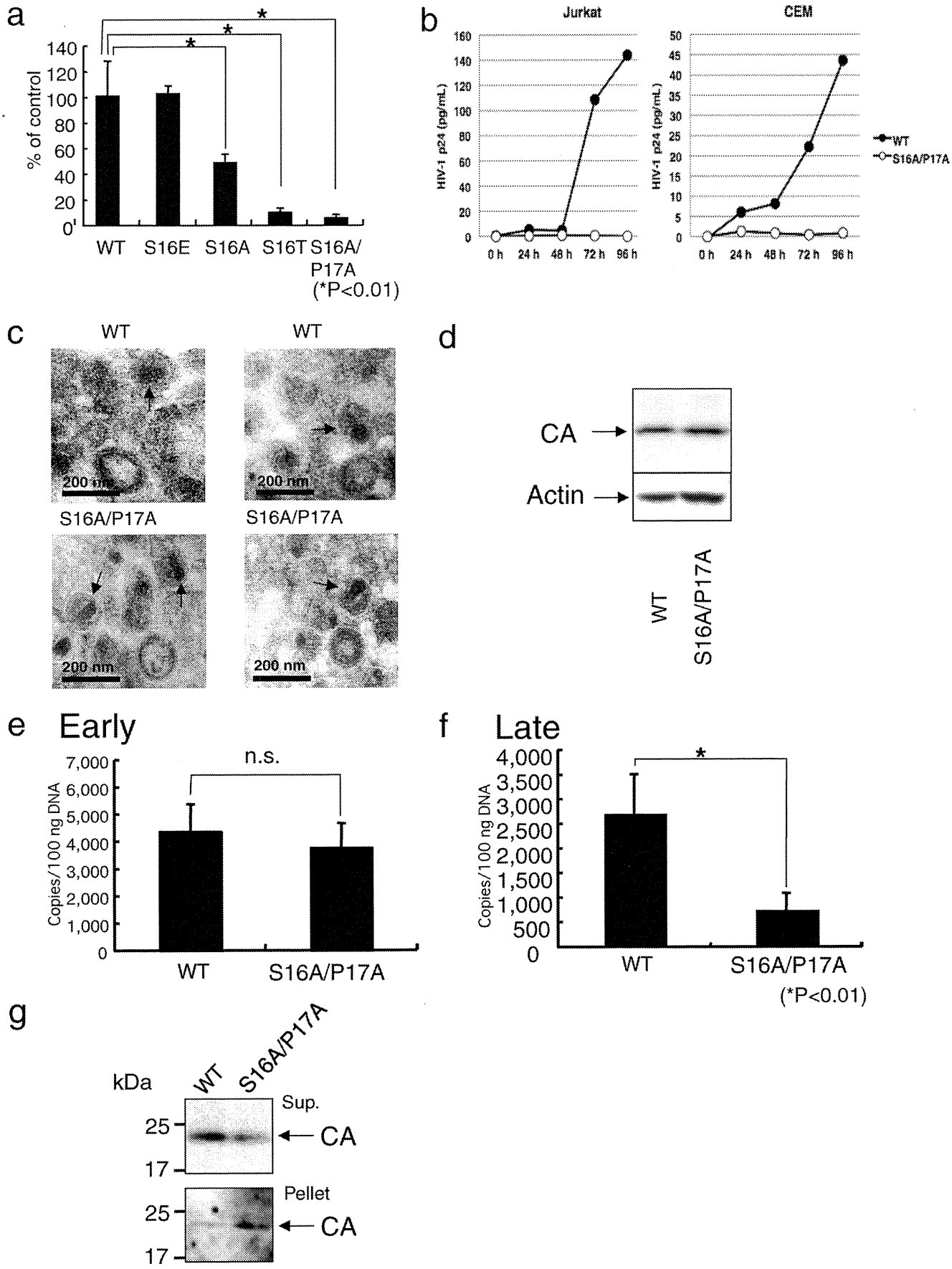

viral infectivity. To examine whether the phenotype of the S16A variant was specific to the selected amino acid changes, we produced another variant with a phosphorylatable amino acid residue, changing Ser to Thr (S16T). The S16T variant showed a remarkably decreased infectivity compared with the WT virus (Fig. 2*a*, $p < 0.01$), suggesting that the Ser^{16} residue in the highly conserved Ser^{16}-Pro^{17} motif (supplemental Fig. S1) plays an important role in maintaining the viral infectivity. To further investigate why Ser^{16} in a fraction of the CA protein in the virion needs to be phosphorylated, we generated another variant (S16A/P17A) because single-point mutations of Ser^{16} in the Ser^{16}-Pro^{17} motif may provide an alternate binding site for conventional peptidyl-prolyl *cis-trans* isomerases, such as cyclophilins, or FK-506-binding proteins, which catalyze the *cis-trans* isomerization of Xaa-Pro peptide bonds (where Xaa is the preceding amino acid) in oligopeptides or proteins. The S16A/P17A variant also had a markedly decreased infectivity in MAGIC-5 cells (Fig. 2*a*, $p < 0.01$) and could not replicate efficiently in T cell lines, Jurkat cells, and CEM cells (Fig. 2*b*), although the core yield of the S16A/P17A variant from HEK293 cells was very similar to that of WT HIV-1, and the phenotypes of the CA core were normal (Fig. 2*c*). Furthermore, to determine whether the lack of infectivity of S16A/P17A was due to a defect in the reverse transcription process, we carried out a viral entry assay and quantitative real time PCR analysis using primers designed to specifically amplify early or late products of reverse transcription. The viral entry assay indicated that the entry levels of S16A/P17A and WT were the same because the amounts of S16A/P17A CA protein in subcellular fractions were very similar to that of WT CA protein (Fig. 2*d*). However, compared with WT, S16A/P17A produced the same level of the early (R/U5) form of the viral cDNA product (Fig. 2*e*) but showed a significant decrease in the level of the late (R/gag) form of the viral cDNA product (Fig. 2*f*, $p < 0.01$). To further examine whether the infectivity defect of the S16A/P17A variant is linked to a dysfunction of uncoating, cell-based fate-of-capsid uncoating assay developed by Sodroski's group (19) was performed. This assay allows us to measure the amounts of cores and soluble free forms of the CA protein present in the cytosol of infected cells. Moreover, the appearance of CA cores in the cytosol inversely correlates with the proper conversion of CA cores to soluble CA in target cells. The amounts of pelletable CA cores in the cells infected with the S16A/P17A mutant virus increased against those detected in the cells infected with WT virus (Fig. 2*g*, *lower panel, Pellet*). Furthermore, the levels of the CA protein in the supernatants from MAGIC-5 cells incubated with the S16A/P17A mutant virus were lower than those detected in the cells infected with WT virus (Fig. 2*g*, *upper panel, Sup.*). These results suggest that the infectivity defect of the S16A/P17A variant is linked to a dysfunction of the uncoating process.

Pin1 within the Target Cell Affects an Early Phase in HIV-1 Replication—Pin1 is a peptidyl-prolyl isomerase that specifically recognizes phosphorylated serine/threonine followed by proline via its WW domain and then catalyzes a conformational change of the bound substrate in a phosphorylation-dependent manner (24, 25). Pin1 has been shown to regulate the stability and localization of its substrates during transcriptional activation, cell cycle progression, and cell death, and a deregulated expression or loss of function of Pin1 leads to the progression of serious human diseases such as cancer and Alzheimer disease (24, 26–28). We therefore considered that Pin1 might bind to and regulate the function of the CA core. We first investigated whether Pin1 directly binds to the CA core by GST-Pin1 pulldown assay. Glutathione beads containing GST or GST-Pin1 were incubated with the CA core purified in accordance with the method described under "Experimental Procedures." To demonstrate that cores were indeed successfully purified, we performed a comparative immunoblot analysis of core preparations. As expected, the membrane-associated matrix (MA) protein (supplemental Fig. S2*a*) and the HIV surface glycoprotein gp120 (supplemental Fig. S2*b*) were substantially depleted in the core preparation. These results indicated that CA core is sufficiently purified. Therefore, in Pin1 pulldown assay, the binding proteins were then analyzed by immunoblotting with an anti-CA antibody. Fig. 3*a* shows that GST-Pin1, but not GST, was bound to the CA core. To investigate whether the binding of the CA core is directly due to the phosphorylation of Ser^{16} in the CA core, WT core particles were treated with ALP or the heat-denatured ALP. The treatment removed phosphate groups from phosphorylated Ser^{16} (Fig. 3*b*) and eliminated the Pin1 binding activity of the CA core (Fig. 3*c*). There are three highly conserved Ser-Pro motifs (Ser^{16}-Pro^{17}, Ser^{33}-Pro^{34}, and Ser^{146}-Pro^{147}) and a conserved Thr^{48}-Pro^{49} motif in the CA protein (supplemental Fig. S1). To examine whether Ser^{33}, Thr^{48}, or Ser^{146} in CA core is phosphorylated, the mixture of CA protein isoforms were subjected to proteome analysis (supplemental Fig. S3). The data demonstrated that Ser^{33}, Thr^{48}, and Ser^{146} in CA core were not phosphorylated. These results suggested that Pin1 binds preferentially to the phosphorylated Ser^{16}-Pro^{17} motif.

Because Pin1 has CA core binding activity, we next determined whether a decrease in endogenous Pin1 expression level decreases HIV-1 infectivity. We transfected MAGIC-5 cells

FIGURE 2. **The S16A/P17A CA mutant shows impaired uncoating process.** *a*, effect of various mutations in Ser^{16}-Pro^{17} motif on viral infectivity. Viral infectivity was determined using MAGIC-5 cells as previously described in Ref. 18. MAGIC-5 cells (1×10^4 cells) were exposed to an equal amount of WT or mutant viruses (corresponding to 3 ng RT). Statistical analysis using the analysis of variance test was performed. The *error bars* denote the standard deviation. *b*, replication kinetics of S16A/P17A variant in Jurkat and CEM cells. *c*, effect of alanine mutation of Ser^{16}-Pro^{17} motif on viral core phenotype. The *arrows* indicate electron-dense cores typical of intact HIV. *d*, effect of alanine mutation of Ser^{16}-Pro^{17} motif on viral entry efficiency. Viral entry assay was performed as described under "Experimental Procedures." *e* and *f*, quantitative analysis of HIV-1 reverse transcription during acute infection using early stage primers (*e*, R/U5) and late stage primers (*f*, R/gag). Briefly, MAGIC-5 cells (1×10^6 cells) were exposed to WT or S16A/P17A virus (2.5 ng of HIV-1 RT) and harvested at 1 day postinfection. The cells were washed with PBS(−), and nucleic acids were extracted. Quantitative analysis was performed using the same primers in accordance with the method of Ikeda *et al.* (17). The significant differences (unpaired *t* test) are indicated as follows: *, $p < 0.01$; *n.s.*, not significant. The *error bars* denote the standard deviation. *g*, effect of Ser^{16}-Pro^{17} motif on fate of CA core in infected cells. MAGIC-5 cells were incubated with WT HIV-1(VSV-G) or S16A/P17A HIV-1(VSV-G) at 4 °C for 30 min and then at 37 °C for 4 h. The cell lysates were analyzed as described under "Experimental Procedures." The supernatants and pellets were Western blotted for CA proteins.

with siRNA against Pin1 or control siRNA. As shown in the *top panel* of Fig. 3*d*, Pin1 siRNA (Pin1 C3) specifically decreased the Pin1 expression level in MAGIC-5 cells without altering actin or lactate dehydrogenase expression level. The cells were infected with HIV-1_{LAV-1}, and β-galactosidase activity was measured as an indicator of infection. In Fig. 3*e*, 60 nM Pin1 siRNA (Pin1 C3)-treated MAGIC-5 cells were infected with HIV-1_{LAV-1} (12 ng of p24 antigen) under the condition in which no HIV-1_{LAV-1}-induced CPE was observed in 60 nM control siRNA-treated MAGIC-5 cells. Interestingly, a decrease in endogenous Pin1 expression level decreased HIV-1_{LAV-1} infectivity (Fig. 3*e*, $p < 0.01$). Furthermore, the effects of Pin1-targeted siRNA treatment on HIV-1 replication were evaluated on the basis of cytopathic effect (*y*) observations (Fig. 3, *f–i*) and quantitative real time PCR analysis using primers designed to specifically amplify late products of reverse transcription. 60 nM

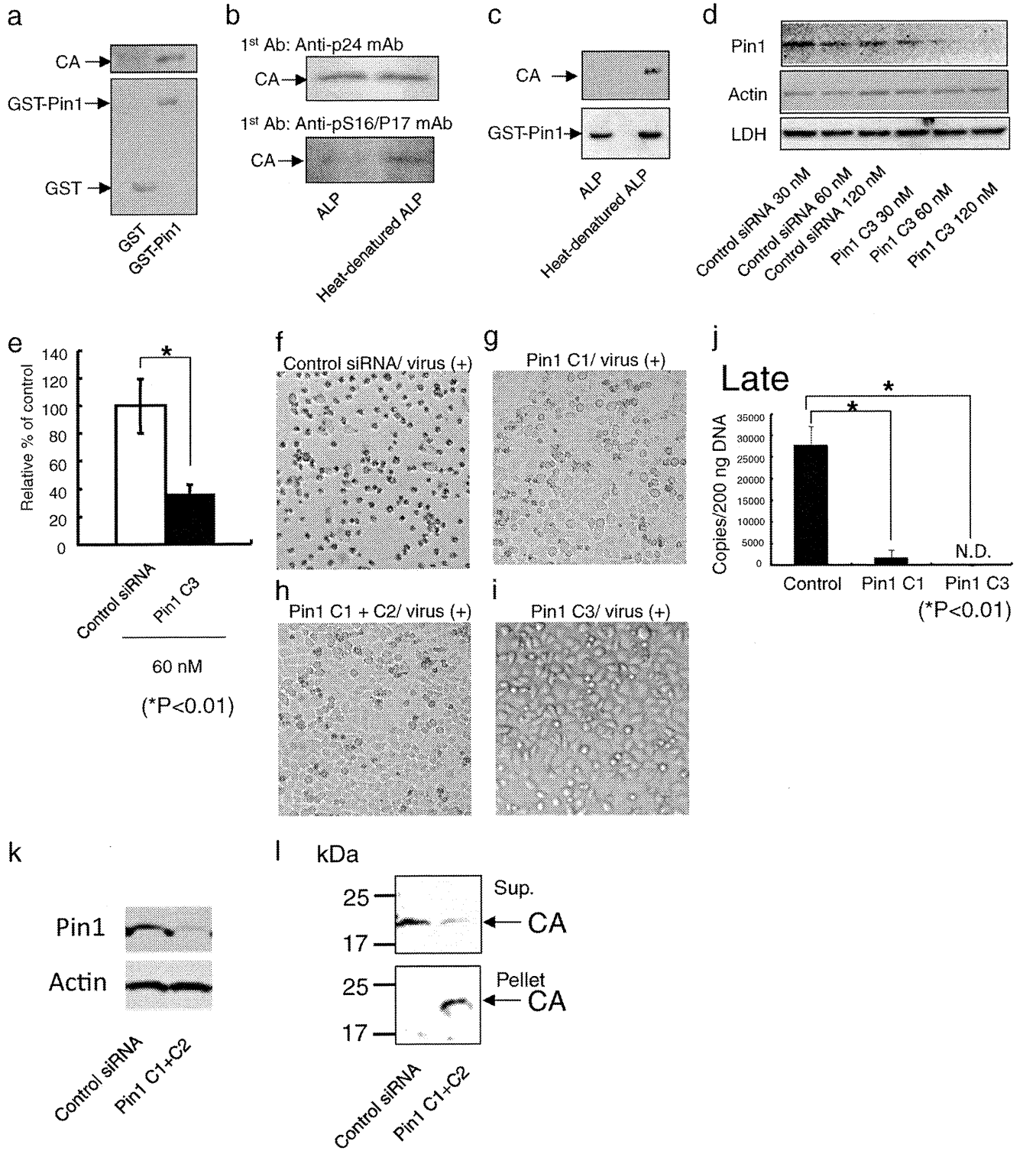

Pin1 C1-, C1+C2-, or C3-treated MAGIC-5 cells was infected with a single-round replication-defective HIV-1 under the condition in which a single-round replication-defective HIV-1-induced CPE was observed in 60 nM control siRNA-treated MAGIC-5 cells (Fig. 3, *f–i*). After treatment with siRNAs, MAGIC-5 cells were infected with single-round replication-defective $HIV_{NL4-3\Delta envWT}$ (11 ng of HIV RT). CPE in infected cells treated with the control siRNA was observed at 46 h postinfection (Fig. 3*f*). On the other hand, CPE was hardly observed in cells treated with 60 nM Pin1 C1, C1+C2, or C3 (Fig. 3, *g–i*, respectively). This indicates that Pin1-targeted siRNAs are capable of inhibiting CPE induced by HIV infection. Furthermore, Fig. 3*j* shows that there was a significant decrease in the level of the late (R/gag) form of the viral cDNA product.

To further examine whether Pin1 depletion is linked to a dysfunction of uncoating, cell-based fate-of-capsid uncoating assay was performed. The amounts of pelletable CA cores in the Pin1 knockdown cells infected with WT HIV-1(VSV-G) increased against those detected in the control siRNA-treated cells infected with WT HIV-1(VSV-G) (Fig. 3, *k* and *l*, *lower panels*, *Pellet*). Furthermore, the levels of the CA protein in the supernatants from the Pin1 knockdown cells infected with WT HIV-1(VSV-G) were lower than those detected in the control siRNA-treated cells infected with the WT HIV-1(VSV-G) (Fig. 3*l*, *upper panel*, *Sup.*). These results indicate that Pin1 depletion is linked to a dysfunction of uncoating.

Pin1 Induces Disassembly of the CA Core—Pin1 might regulate the uncoating of the CA core. To test this possibility, we attempted to study this process *in vitro* by detecting the disassembly of the CA core in the presence of Pin1. Purified CA cores were diluted with an uncoating assay buffer and incubated with GST-Pin1, heat-denatured, inhibitor-treated, or W34A/K63A GST-Pin1. Following incubation, the CA cores were subjected to ultracentrifugation to separate the free CA protein from the intact CA core. CA core dissociation was found to be GST-Pin1-dependent (Fig. 4*a*, *lane 2*), and the effect was attenuated when Pin1 was denatured (Fig. 4*b*, $p < 0.01$) or treated with the Pin1 inhibitor juglone (Fig. 4*c*, $p < 0.01$) and catalytically inactived the W34A/K63A Pin1 mutant (Fig. 4*d*, $p < 0.01$). Furthermore, the uncoating assay demonstrated that the Pin1-dependent disassembly was competed with the anti-pS16/P17 serum (Fig. 4*e*, $p < 0.01$) and blocked by the pretreatment of the core with ALP (Fig. 4*e*, $p < 0.01$). These results support the idea that Pin1 facilitates the HIV-1 uncoating by interacting with the CA core.

DISCUSSION

Much is known about the structure of the HIV-1 CA protein (29–31), but the mechanism and requirement of HIV-1 uncoating in postentry events have remained poorly defined. However, recent studies showed that the HIV-1 uncoating activity, which releases the CA protein from HIV-1 cores and is required for the activation of reverse transcriptase, is due to cellular factors (3, 4). The studies suggest that the ordered uncoating process of HIV-1 is not spontaneous and is regulated by cellular factors. Therefore, we employed a series of biochemical approaches to clarify the mechanism of HIV-1 CA core uncoating.

In this study, we showed that Pin1 assists the uncoating of the HIV core. Proteome analysis suggests that the Ser residue in the Ser[16]-Pro[17] motif of CA-a is preferentially phosphorylated (Fig. 1, *c* and *d*). Interestingly, three Ser-Pro motifs (Ser[16]-Pro[17], Ser[33]-Pro[34], and Ser[146]-Pro[147]) are highly conserved across HIV-1 clades (supplemental Fig. S1), and only the Ser[16]-Pro[17] motif is conserved among HIV-1, HIV-2, and simian immunodeficiency virus (SIV) (supplemental Fig. S4). As shown in Figs. 2*g* and 3*l*, cell-based fate-of-capsid uncoating assay demonstrated that the infectivity defect of the S16A/P17A variant is linked to a dysfunction of the uncoating process, and Pin1 depletion in the target cells is linked to a dysfunction of uncoating. Furthermore, GST-Pin1 pulldown assay and *in vitro* uncoating assay indicated that Pin1 facilitates HIV-1 uncoating by interacting with the CA core through the Ser[16]-Pro[17] motif (Figs. 3, *b* and *c*, and 4, *e* and *f*). These results suggest that only a fraction of the CA protein phosphorylated at Ser[16]-Pro[17] motif serves as a molecular switch to signal CA core uncoating because both the assembly and disassembly pathways cannot act on the CA core at the same time.

To investigate how the motif of CA-a is phosphorylated, Western immunoblot analysis with monoclonal anti-pS16/P17 mAb was carried out, which demonstrated that Ser[16] was phosphorylated inside $HIV\text{-}1_{LAV\text{-}1}$ virions but not inside CEM/LAV-1 cells, although the specific kinase that phosphorylates Ser[16] is currently unknown (supplemental Fig. S5). As shown in Fig. 3*e*, a decrease in endogenous Pin1 expression level decreases HIV-1 infectivity. These findings suggest that the CA

FIGURE 3. **Interactions of Pin1 with the CA core and Pin1 within the target cells regulate HIV-1 infectivity.** *a*, the CA core was subjected to GST-Pin1 pulldown assay and immunoblotted with anti-p24 mAb (*upper panel*). CBB staining of GST and GST-Pin1 (*lower panel*). *b*, treatment of CA core with ALP or heat-denatured ALP. The ALP- and heat-denatured ALP-treated CA cores were subjected to Western immunoblot analysis using anti-pS16/P17 mAb or anti-p24 mAb. The treatment removed phosphate groups from phosphorylated Ser[16]. *c*, effect of ALP on interaction between Pin and CA core. The ALP-treated CA core was subjected to GST-Pin1 pulldown assay and immunoblotted with anti-p24 mAb (*upper panel*). CBB staining of GST-Pin1 is shown (*lower panel*). *d* and *e*, the suppression of Pin1 expression by 60 nM Pin1 C3 siRNA (*d*, *upper panel*, the expressions of actin and lactate dehydrogenase (*LDH*) were not affected by Pin1-specific siRNA)) in MAGIC-5 cells (1×10^4 cells) results in an attenuated $HIV\text{-}1_{LAV\text{-}1}$ replication (*e*). The significant differences (unpaired *t* test) are indicated as follows: *, $p < 0.01$. The *error bars* denote the standard deviation. *f–i*, the effects of Pin1-specific siRNAs were evaluated on the basis of CPE observations. The cells (2×10^5 cells) were pretreated with 60 nM control siRNA (*f*), Pin1 C1 (*g*), Pin1 C1+C2 (*h*), and Pin1 C3 (*i*) and then infected with single-round replication-defective HIV-1 ($HIV_{NL4-3\Delta envWT}$). Pin1-specific siRNAs were capable of inhibiting CPE induced by HIV infection. *j*, effect of Pin1 siRNAs on reverse transcription. The knockdown of Pin1 showed that there was a significant decrease in the level of the late (R/gag) form of the viral cDNA product. Statistical analysis using the analysis of variance test was performed. The *error bars* denote the standard deviation. *N.D.*, not detected. The detection limit of late products of HIV-1 reverse transcription was 400 copies/reaction in the assay. *k*, Pin1 C1+C2-induced suppression of Pin1 expression. MAGIC-5 cells were transfected with Pin1 C1+C2 siRNA (600 nM) using the Neon™ transfection system (*upper panel*, the expression of actin was not affected by Pin1 C1+C2). *l*, effect of Pin1 depletion on fate of CA core in infected cells. Pin1 knockdown cells treated with Pin1 C1+C2 siRNA were incubated with WT HIV-1(VSV-G) at 4 °C for 30 min and then at 37 °C for 4 h. The cell lysates were analyzed as described under "Experimental Procedures." The supernatants and pellets were analyzed by Western blotting for the CA proteins.

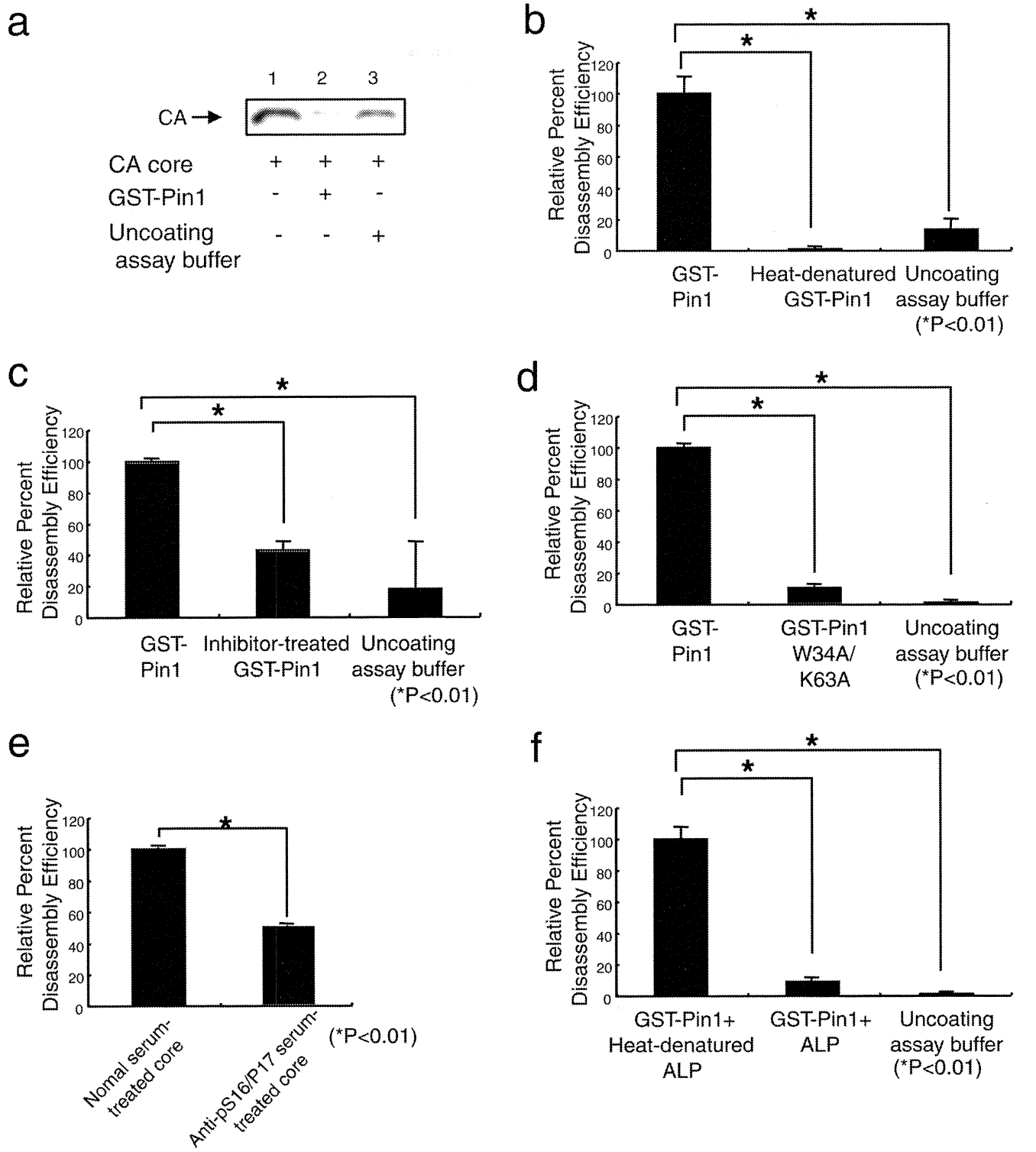

FIGURE 4. ***In vitro* uncoating of CA core by GST-Pin1.** *a*, *in vitro* uncoating assay was performed as described under "Experimental Procedures." The extent of uncoating was visualized by Western blot analysis using anti-p24 mAb after the undisassembled cores have been pelleted in an ultracentrifuge. CA cores in the presence of GST-Pin1 disassembled *in vitro* (*lane 2*). The quantities of the CA protein in the pellets in the presence of uncoating assay buffer were similar to that of the input CA protein (*lanes 1* and *3*). *b*, after incubating HIV-1 cores with GST-Pin1, heat-denatured GST-Pin1, or uncoating assay buffer for 1 h, the relative percentage of disassembly efficiency is given by the equation shown under "Experimental Procedures." Pin1 induces disassembly of the CA cores. *c*, *in vitro* uncoating activities after incubating HIV-1 cores with juglone-treated Pin1 for 1 h. The treatment of GST-Pin1 with juglone results in an attenuated *in vitro* uncoating. *d*, effect of GST-Pin1 (W34A/K63A) on uncoating. *In vitro* uncoating activities after incubating GST-Pin1 (W34A/K63A) with CA cores for 1 h. *e*, *in vitro* competitive uncoating assay. The pretreatment of CA cores with anti-pS16/p17 serum results in an attenuated *in vitro* uncoating. *f*, *in vitro* uncoating activities after incubating HIV CA cores with ALP for 2 h. Pin1-dependent disassembly was blocked by the pretreatment of the cores with ALP. *b–f*, statistical analysis using the analysis of variance test was performed. The *error bars* denote the standard deviation. The significant differences are indicated as follows: *, $p < 0.01$.